Article

Attenuated effector T cells are linked to control of chronic HBV infection

Kathrin Heim[1,2,14], Sagar [1,2,14], Özlem Sogukpinar[1,2], Sian Llewellyn-Lacey[3], David A. Price [3,4], Florian Emmerich[2,5], Anke R. M. Kraft [6,7,8,9], Markus Cornberg[6,7,8,9], Sophie Kielbassa[1,2], Percy Knolle [10,11,12], Dirk Wohlleber [10], Bertram Bengsch [1,2,13], Tobias Boettler [1,2], Christoph Neumann-Haefelin [1,2], Robert Thimme [1,2,15] ✉ & Maike Hofmann [1,2,15] ✉

Hepatitis B virus (HBV)-specific CD8+ T cells play a dominant role during acute-resolving HBV infection but are functionally impaired during chronic HBV infection in humans. These functional deficits have been linked with metabolic and phenotypic heterogeneity, but it has remained unclear to what extent different subsets of HBV-specific CD8+ T cells still suppress viral replication. We addressed this issue by deep profiling, functional testing and perturbation of HBV-specific CD8+ T cells during different phases of chronic HBV infection. Our data revealed a mechanism of effector CD8+ T cell attenuation that emerges alongside classical CD8+ T cell exhaustion. Attenuated HBV-specific CD8+ T cells were characterized by cytotoxic properties and a dampened effector differentiation program, determined by antigen recognition and TGFβ signaling, and were associated with viral control during chronic HBV infection. These observations identify a distinct subset of CD8+ T cells linked with immune efficacy in the context of a chronic human viral infection with immunotherapeutic potential.

Chronic HBV infection is a highly relevant disease with approximately 257 million infected people worldwide resulting in 887,000 deaths per year due to the development of progressive liver disease and hepatocellular carcinoma[1]. Clinically, chronic HBV infection seems quite variable in different clinical phases. The clinical phases of chronic HBV infection can be principally divided into two categories: (1) chronic hepatitis B (CHB) characterized by the presence of liver pathology and (2) chronic HBV infection without signs of liver injury (endogenous control). The World Health Organization and clinical guidelines recommend that patients who are chronically HBV-infected with high viral loads (VLs) and/or liver injury receive nucleos(t)ide analog (NUC) treatment to abrogate viral replication and thus immediately reduce viral burden[1,2]; however, with NUC treatment a cure is not achieved and therefore long-term therapy is required. Hence, chronic HBV infection with a low VL can either be endogenously controlled or mediated by NUC treatment (NUC control).

HBV-specific CD8+ T cells play a dominant role in the outcome of HBV infection and have been linked to both viral control and disease pathogenesis during acute infection[3,4]. During chronic HBV infection, altered HBV-specific T cell responses have been reported in the different clinical phases. They are characterized by low abundance, impaired cytokine production, limited expansion capacity, high TOX expression, low T-BET expression and an altered metabolism, which are all characteristics of exhausted T (T_EX) cells [5–11]. Of note, T cell exhaustion represents a distinct T cell differentiation program of functional adaptation to persisting antigen recognition. The molecular mechanisms underlying T cell exhaustion have been mainly established in mouse models of chronic lymphocytic choriomeningitis virus (LCMV) infection[12,13]; however, many features of T cell exhaustion could be translated to the human system, for example expression of inhibitory receptors such as PD1 and a transcriptional program reflected by high TOX and EOMES but low T-BET expression, as shown for virus-specific

CD8^{+} T cells in chronic HBV and hepatitis C virus (HCV) infection[11,14,15]. Still, it is not fully elucidated whether the T cell exhaustion program covers all facets of T cell responses in chronic viral infections in humans.

In mice and humans, there is also growing evidence that exhausted T cells do not represent a uniform but rather heterogeneous population consisting of several subsets within two main groups: PD1^{int} progenitor/precursor/memory-like subsets and PD1^{hi} terminal exhausted subsets[16]. Progenitor/precursor/memory-like subsets are characterized by the transcription factor TCF1 and give rise to the terminal exhausted T cells through antigen-driven proliferation[17]. In humans, especially HBV-specific CD8^{+} T cells have also been shown to be heterogeneous with respect to their phenotypic, functional and metabolic characteristics[18–22]. One determinant of HBV-specific CD8^{+} T cell heterogeneity is the targeted antigen with HBV envelope-specific CD8^{+} T cells being hardly detectable in comparison to HBV core- and HBV polymerase-specific CD8^{+} T cells that are more abundant in the blood[18,19]. Additionally, HBV core- and HBV polymerase-specific CD8^{+} T cells differ in phenotype and function[18,19]. The relevance of T cell heterogeneity has been underpinned by an association of certain HBV-specific CD8^{+} T cell responses with successful therapy[23]; however, the contribution of HBV-specific T cell heterogeneity to the clinical course and thus a distinct clinical phase of chronic infection has not been analyzed in detail. Here, by using single-cell RNA sequencing (scRNA-seq) we analyzed the molecular heterogeneity of HBV-specific CD8^{+} T cells in different clinical phases. We identified a program of T cell attenuation with its TGFβ-involving mechanistic underpinnings in parallel to classical T cell exhaustion in a chronic human viral infection. T cell attenuation was linked to endogenous viral control highlighting the clinical relevance of different facets of HBV-specific T cell programming in chronic viral infection.

Results

HBV-specific CD8^{+} T cell heterogeneity

First, to analyze the transcriptional heterogeneity of HBV-specific CD8^{+} T cells obtained from patients who are chronically HBV-infected (hepatitis B e-antigen negative (HBeAg−) disease phases/treated and nontreated, low VL; $n = 14$) in an unbiased approach, we performed single-cell RNA sequencing (scRNA-seq) analysis using the mCEL-seq2 protocol[24] (Extended Data Fig. 1a,b). As a reference population of human T_{EX} cells, we included HCV-specific CD8^{+} T cells obtained from patients with HCV infection, either chronically infected ($n = 6$) or cured by directly acting antivirals (DAAs) ($n = 2$)[25]. Cluster analysis applying the Seurat and Harmony algorithm to single-cell transcriptomes[26,27] of 1,954 HBV-specific and 818 HCV-specific CD8^{+} T cells revealed the existence of five different cell clusters (Fig. 1a). Differentially expressed genes (DEGs) comparing these five clusters included *IL7R, TCF7, GZMB, TGFBR3, NR4A2, CD38, EZH2* and *TOX* thus covering cytokine responsiveness, epigenetic remodeling, activation, proliferative and functional characteristics (Fig. 1b). Specifically, cluster 2 was characterized by a memory-like signature, whereas cluster 4 exhibited a profile of terminal T cell exhaustion as also confirmed by gene set enrichment analysis (GSEA) applying gene signatures of T_{EX}, memory T cells and memory-like T cells obtained from the LCMV mouse model[17] (Fig. 1b,c). Additionally, cluster 1 showed a gene signature that classifies

cytotoxic effector cells (*GZMB, GNLY, PRF1, KLRG1, CX3CR1, TBX21* and *ZEB2*) distinct from the recently described STAT5-dependent, KLRC/ B1-expressing effector-like T_{EX} cells[28,29] (Fig. 1b and Extended Data Fig. 1c). Clusters 0 and 3 displayed overlaps with effector/memory signatures (*ID2, ID3, TNF* and *ZEB1*) according to the human T cell differentiation Atlas[30] (Fig. 1d). Next, we linked these clusters to CD8^{+} T cells targeting HBV versus HCV and observed clearly differential cluster distribution with a unique pattern of heterogeneity of HBV-specific CD8^{+} T cells (Fig. 1e). In particular, cluster 4 was strictly dominated by HCV-specific CD8^{+} T_{EX} cells obtained from the chronic phase of HCV infection (Fig. 1f). HBV- and HCV-specific CD8^{+} T cells contributed nearly equally to clusters 2 and 3 reflecting memory-like profiles as observed in HCV infection after DAA-mediated cure (Fig. 1f); however, HBV-specific CD8^{+} T cells additionally dominate the cytotoxic cluster 1 and cluster 0 with hardly any HCV-specific CD8^{+} T cell found within these two clusters. Hence, HBV-specific CD8^{+} T cell heterogeneity exceeds HCV-specific CD8^{+} T cell heterogeneity in chronic infection by the presence of cell clusters distinct from terminal T_{EX} and memory-like T_{ML} cells.

Cytotoxic CD8^{+} T cells target HBV pol in chronic infection

We and others have previously shown that the targeted antigen is a major determinant of HBV-specific CD8^{+} T cell phenotype and function[18,19,21]. To investigate the impact of the targeted antigen on the transcriptional heterogeneity and subset diversification, we performed clustering analysis to single-cell transcriptomes of 1,056 HBV core[18]-specific ($n = 7$ patients who were chronically HBV-infected) and 1,284 HBV pol[455]-specific CD8^{+} T cells ($n = 7$ patients who were chronically HBV-infected). We identified four clusters (Fig. 2a) that again revealed differential expression of, for example, *NR4A2, GZMB, TGFBR3* and *IL7R* and thus cover memory and cytotoxic characteristics and different cytokine responsiveness. Cluster 1 was enriched in genes indicative of cytotoxicity, whereas cluster 2 showed an overlapping effector/memory gene signature and clusters 3 and 0 were enriched for signature genes of memory-like/memory T cells, respectively (Fig. 2b). Clusters 3, 2 and 0 were rather equally composed of HBV core[18]- and HBV pol[455]-specific CD8^{+} T cells; however, HBV pol[455]-specific CD8^{+} T cells dominated the cytotoxic cluster 1 (Fig. 2c). In addition to the cytotoxic signature[25], cluster 1 also revealed an enrichment of genes involved in T cell cytokine production (Fig. 2d) complementing the effector cell potential of this HBV pol[455]-specific CD8^{+} T cell subset. Of note, single cytokines were only lowly expressed at the transcript level in our scRNA-seq dataset of virus-specific CD8^{+} T cells (Extended Data Fig. 1d). Different subset diversification of HBV core[18]- versus HBV pol[455]-specific CD8^{+} T cells was confirmed at the protein level after concatenating flow cytometric expression analysis of GZMB, PRF1, KLRD1, NKG7, TOX, PD1, T-BET, EOMES and CD127 of all HBV-specific CD8^{+} T cells and dimensionality reduction using *t*-distributed stochastic neighbor embedding (*t*-SNE) (Fig. 2e). Again, a large fraction of HBV pol[455]-specific CD8^{+} T cells expressed marker molecules of cytotoxicity and effector cell differentiation. Of note, protein expression analysis also revealed a marked expression of CD127 required for T cell maintenance in these cells (Fig. 2e). Taken together, these results identified a cytotoxic HBV pol[455]-specific CD8^{+} T cell subset during chronic infection with typical features of effector cells devoid of hallmarks of T cell exhaustion.
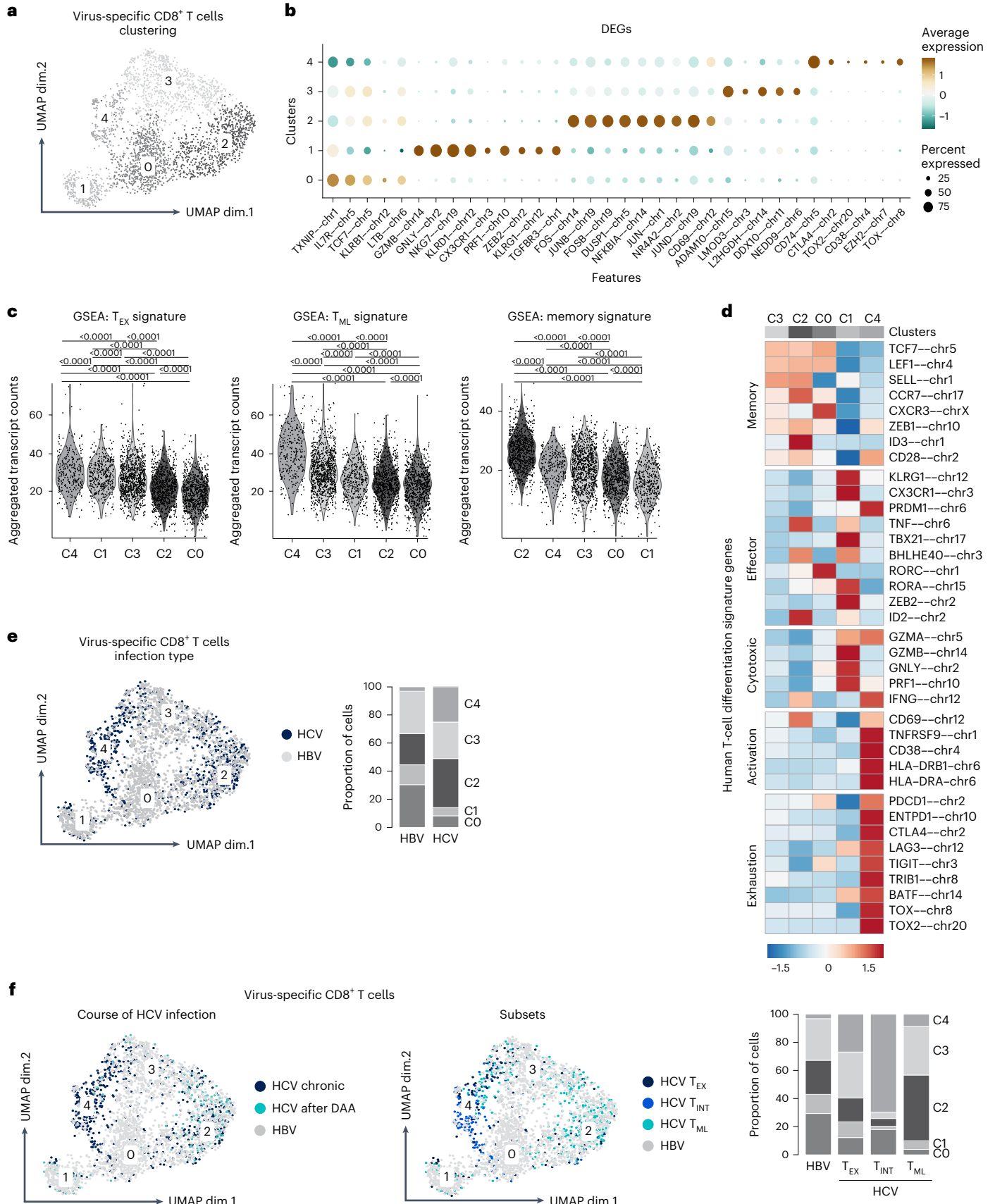

Fig. 1 | Subset diversification of virus-specific CD8^{+} T cells in chronic viral hepatitis. a, Cluster analysis via Seurat and Harmony algorithm applied to single-cell transcriptomes of HBV- ($n = 14$) and HCV-specific CD8^{+} T cells ($n = 8$). Each dot corresponds to one individual cell. Five clusters (C0–C4) were identified and color coded. **b**, Bubble plot of DEGs among the five clusters is displayed. Scaled expression is depicted. **c**, GSEA of terminally exhausted, memory-like and classical memory murine T cell signatures (from ref. 17) comparing C0–C4. Violin plots depict the aggregated transcript counts. Statistical significance was assessed by a Kruskal–Wallis test, including Dunn's multiple comparisons test. **d**, Heatmap showing human T cell differentiation signature gene expression

(memory, effector, cytotoxic, activation and exhaustion) in C0–C4. Scaled expression levels are color coded (blue, low; red, high). **e**, C0–4 are color coded according to infection type (dark blue, HCV; gray, HBV) and the proportion of each cluster was assessed for HBV- and HCV-specific CD8^{+} T cells, respectively. **f**, HCV-specific CD8^{+} T cells were highlighted with respect to the course of HCV infection (dark blue, HCV chronic; light blue, HCV after DAA; gray, HBV) or with respect to distinct T cell subsets (dark blue, HCV T_{EX} cells; dark blue/gray, HCV T_{INT}; light blue, HCV T_{ML}; gray, HBV) and the proportions were assessed for each cluster. T_{ML}, memory-like T cells; T_{INT}, intermediate exhausted T cells.

Cytotoxic CD8⁺ T cells are linked to endogenous HBV control

To further investigate the biological relevance of the identified cytotoxic CD8⁺ T cell population in chronic HBV infection, we compared the transcriptional profile of HBV pol$_{455}$-specific CD8⁺ T cells in patients with chronic HBV infection who endogenously control the virus (HBeAg− cHBV infection) and do not require antiviral therapy versus patients with CHB requiring antiviral NUC therapy (NUC-treated HBeAg− CHB/; NUC control). Cluster analysis to single transcriptomes
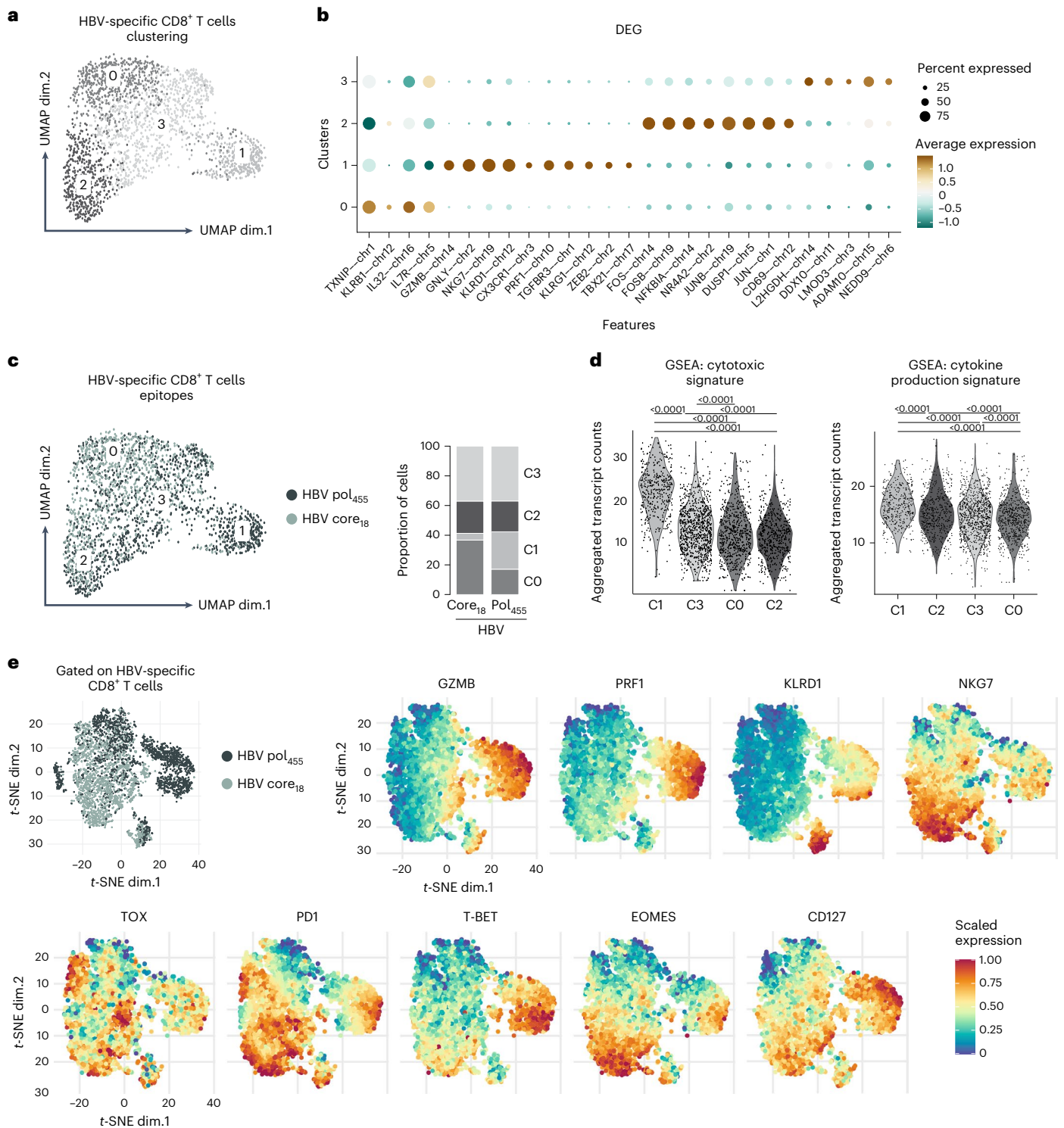

a, Virus-specific CD8⁺ T cells clustering

b, DEGs

c, GSEA: T$_{EX}$ signature; GSEA: T$_{ML}$ signature; GSEA: memory signature

d, Human T-cell differentiation signature genes

e, Virus-specific CD8⁺ T cells infection type

f, Virus-specific CD8⁺ T cells; Course of HCV infection; Subsets

Fig. 2 | Distinct subsets of HBV core$_{18}$- and HBV pol$_{455}$-specific CD8$^+$ T cells. **a**, Cluster analysis via Seurat and Harmony algorithm applied to single-cell transcriptomes of HBV core$_{18}$-specific ($n = 7$) versus HBV pol$_{455}$-specific ($n = 7$) CD8$^+$ T cells of individuals who were chronically HBV-infected (HBeAg−, low VL). Each dot corresponds to one cell. Four clusters (C0–3) were identified and color coded. **b**, Bubble plot showing DEGs in C0–C3. Scaled expression is depicted. **c**, C0–3 are color coded according to targeted viral proteins (light gray/green, HBV core$_{18}$; dark green/gray, HBV pol$_{455}$). Proportions of C0–C3 among HBV-specific CD8$^+$ T cells are illustrated. **d**, GSEA of cytotoxicity (from ref. 25) and cytokine production (GO:0002369) signatures are depicted. The aggregated transcript counts of C0–3 are mapped. Statistical significance was assessed by a Kruskal–Wallis test, including Dunn's multiple comparisons test. **e**, t-SNE representation of concatenated flow cytometry data comparing HBV core$_{18}$- versus HBV pol$_{455}$-specific CD8$^+$ T cells is illustrated (HBV core$_{18}$, $n = 25$; HBV pol$_{455}$, $n = 26$). Expression levels (blue, low; red, high) of the indicated markers are plotted.

of 595 HBV pol$_{455}$-specific CD8$^+$ T cells obtained from three patients with endogenous control and of 689 HBV pol$_{455}$-specific CD8$^+$ T cells obtained from four patients with NUC control revealed the existence

of three different cell clusters, including a prominent cytotoxic cluster 1 characterized by *GNLY*, *GZMB*, *PRF1* and *NKG7* expression (Fig. 3a). These HBV pol$_{455}$-specific CD8$^+$ T cells with a cytotoxic signature were
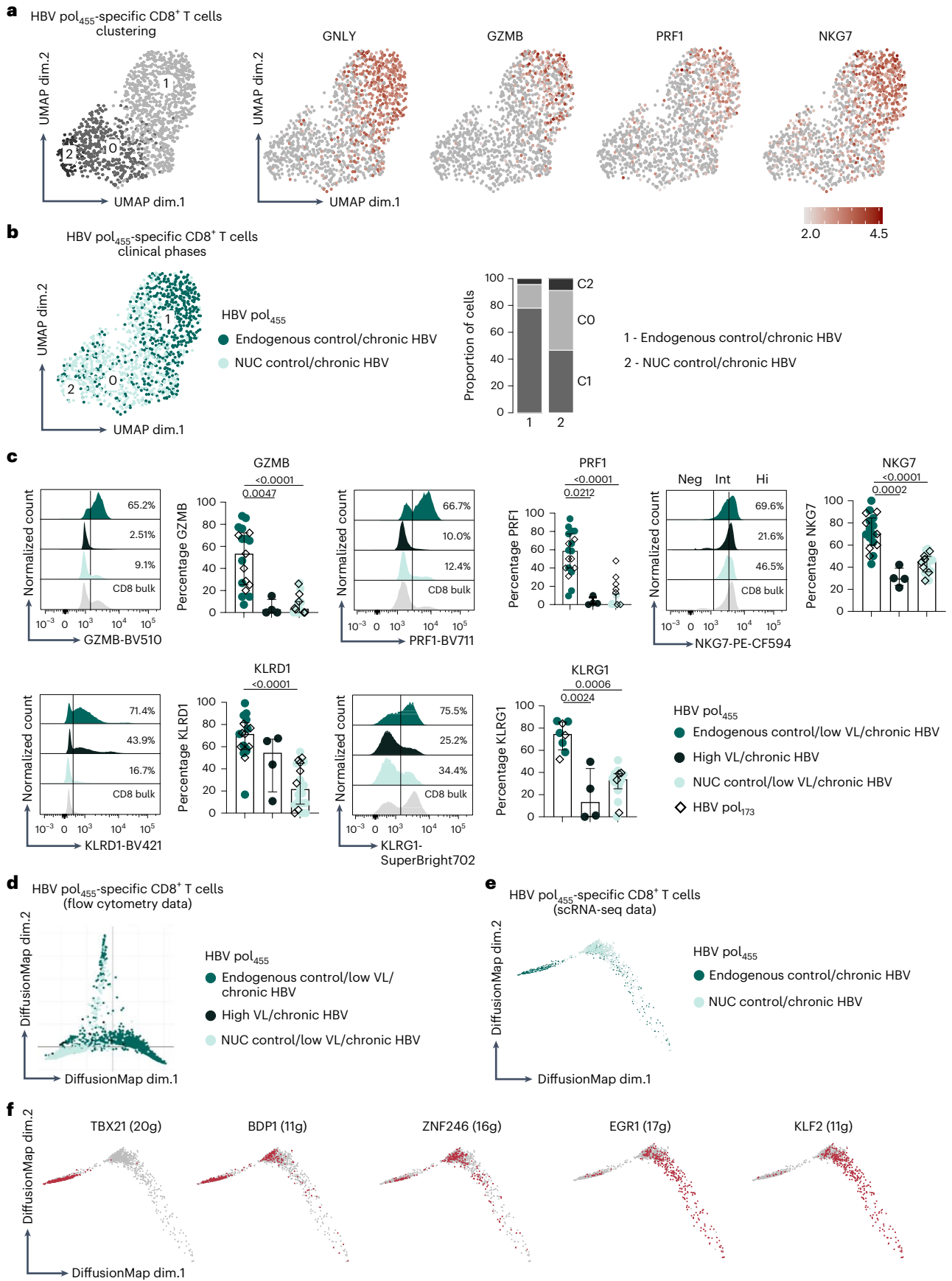
Fig. 3 | Cytotoxic HBV pol$_{455}$-specific CD8$^+$ T cells are associated with endogenous control in chronic HBV infection. a, Cluster analysis via Seurat and Harmony algorithm applied to single-cell transcriptomes of HBV pol$_{455}$-specific CD8$^+$ T cells obtained from chronic HBV-infected individuals with endogenous control/chronic HBV (n = 3) versus NUC control/chronic HBV (n = 4). Each dot corresponds to one individual cell. Three clusters (C0–2) were identified and color coded. Feature plots showing gene expression of cytotoxic genes among the three clusters and scaled expression (gray, low; red, high) are depicted. **b**, C0–2 are color coded according to the clinical phase of chronic HBV infection (dark green, endogenous control; light green, NUC control) and proportions of C0–2 of HBV pol$_{455}$-specific CD8$^+$ T cells were assessed. **c**, Flow cytometric analysis of the cytotoxic molecules GZMB and PRF1, the cytolytic regulator NKG7 as well as the C-type lectin-like natural killer cell receptors KLRD1 and KLRG1 in HBV pol$_{455/173}$-specific CD8$^+$ T cells from chronic HBV-infected individuals (for GZMB, PRF1, NKG7, KLRD1: endogenous control/chronic HBV (low VL, HBV pol$_{455}$: n = 12, HBV pol$_{173}$: n = 7), chronic HBV/high VL (HBV pol$_{455}$: n = 4), NUC control/ chronic HBV (low VL, HBV pol$_{455}$: n = 14, HBV pol$_{173}$: n = 7; for KLRG1: endogenous control/chronic HBV (low VL, HBV pol$_{455}$: n = 5, HBV pol$_{173}$: n = 3), chronic

HBV/high VL (HBV pol$_{455}$: n = 4) NUC control/chronic HBV (low VL, HBV pol$_{455}$: n = 9, HBV pol$_{173}$: n = 3)). Histograms and statistical graph depicting gating and frequencies of HBV pol$_{455/173}$-specific CD8$^+$ T cells are displayed. Each dot represents one HBV pol$_{455/173}$-specific CD8$^+$ T cell and is color coded as indicated: dark green, endogenous control/chronic HBV; dark gray green, chronic HBV/high VL; light green, NUC control/chronic HBV. Bar charts show the median value with interquartile range (IQR). **d**, Diffusion map showing flow cytometry data of HBV pol$_{455}$-specific CD8$^+$ T cells according to the clinical phase of chronic HBV infection is depicted (endogenous control/chronic HBV, n = 12; chronic HBV/high VL, n = 4; NUC control/chronic HBV, n = 14). **e**, Diffusion pseudotime (DPT) trajectory of the single-cell transcriptomes of HBV pol$_{455}$-specific CD8$^+$ T cells is shown. Each dot represents one cell and these are color coded according to clinical phase of chronic HBV infection endogenous control/chronic HBV (n = 3) versus NUC control/chronic HBV (n = 4). **f**, Binary regulon activity of HBV pol$_{455}$-specific CD8$^+$ T cells is plotted on diffusion map based on SCENIC analysis. Cells are colored in red when the indicated regulon is active. Statistical significance was assessed by a Kruskal–Wallis test, including Dunn's multiple comparisons test (**c**).

strongly associated with endogenous control (Fig. 3b). In contrast, clusters 0 and 2 primarily consisted of HBV pol$_{455}$-specific CD8$^+$ T cells obtained from NUC control patients (Fig. 3b), expressing memory markers such TCF1 and interleukin (IL)-7R (Extended Data Fig. 2a). To confirm that the absence of the cytotoxic signature in HBV pol$_{455}$-specific CD8$^+$ T cells obtained from NUC-treated patients is indeed linked to the absence of viral control before therapy, we flow cytometrically analyzed HBV pol$_{455}$-specific CD8$^+$ T cells from patients with HBeAg− CHB and high VLs before initiation of NUC therapy (high VL/chronic HBV). Similar to NUC-treated patients and in contrast to patients with endogenous control, HBV pol$_{455}$-specific CD8$^+$ T cells obtained from patients before NUC treatment exhibited reduced expression of GZMB, PRF, NKG7, KLRD1 and KLRG1 (Fig. 3c) as it was also the case for HBV core$_{18}$-specific CD8$^+$ T cells in all tested clinical phases of chronic HBV infection (Extended Data Fig. 2b). It is important to note that this association of cytotoxicity and endogenous control is protein (polymerase/ pol)- and not epitope-specific as a similar differential expression of cytotoxic molecules was also present in HBV pol$_{173}$-specific CD8$^+$ T cells (Fig. 3c). In addition, we conducted diffusion pseudotime (DPT) analysis[31] of concatenated flow cytometric data, including CD127, PD1, TOX, GZMB, PRF1, KLRD1, NKG7, ZEB2, T-BET and EOMES expression of HBV pol$_{455/173}$-specific CD8$^+$ T cells from HBeAg− CHB, NUC control and endogenous control patients (Fig. 3d and Extended Data Fig. 2c). The subsets were residing on a two-dimensional manifold with two branches reflecting diverging trajectories in endogenous control versus CHB/NUC control phases of chronic HBV infection (Fig. 3d). Next, to gain further insights into the differential transcriptional regulation of the HBV pol$_{455}$-specific CD8$^+$ T cell response in endogenous versus NUC control patients, we performed DPT analysis of the scRNA-seq data. Again, HBV pol$_{455}$-specific CD8$^+$ T cells allocated in a two-dimensional

manifold with two branches separating subsets obtained from endogenous versus NUC control patients (Fig. 3e). Gene regulatory network inference using SCENIC[32] revealed that cytotoxic HBV pol$_{455}$-specific CD8$^+$ T cells from endogenous control patients were characterized by TBX21, BDP1, ZNF246, POLR2A, ATF4 and CREM activity, whereas HBV pol$_{455}$-specific CD8$^+$ T cells from NUC control patients exhibited higher activity of EGR1, KLF2 and AP-1 transcription factors (Fig. 3f and Extended Data Fig. 2d). These data indicate a memory-like/progenitor exhausted state of circulating HBV pol$_{455}$-specific CD8$^+$ T cells in NUC control patients. In contrast, cytotoxic HBV pol$_{455}$-specific CD8$^+$ T cells showed a signature of transcriptionally active effector T cells. Hence, the selective presence of cytotoxic HBV pol$_{455}$-specific CD8$^+$ T cells in patients with endogenous control strongly supports a biological relevant link between this subset and immune-mediated HBV control in chronic infection.

Attenuated cytotoxic CD8$^+$ T cell response in the chronic HBV phase

The presence of a clinically relevant cytotoxic CD8$^+$ T cell subset during endogenously controlled chronic HBV infection prompted us to investigate whether this HBV-specific T cell response is similar to an effector T cell response in acute-resolving infection. We compared the HBV pol$_{455}$-specific CD8$^+$ T cell response in 7 acutely HBV-infected versus 26 chronically infected, endogenously controlled patients versus 5 patients who spontaneously resolved an acute HBV infection. The frequency (Fig. 4a) and activation status as reflected by higher Ki67 and CD38 expression (Fig. 4b) of HBV pol$_{455}$-specific CD8$^+$ T cells was higher in patients with acute HBV versus endogenously controlled chronic infection; however, the HBV pol$_{455}$-specific CD8$^+$ T cell response in patients with endogenous control was marked by an increase in

Fig. 4 | Attenuated cytotoxic HBV pol$_{455}$-specific CD8$^+$ T cell response. a, Dot plots show circulating peptide/HLA-A*02:01 tetramer-enriched HBV pol$_{455}$-specific CD8$^+$ T cells in endogenous control/chronic HBV (left, n = 20), acute HBV (middle, n = 7) and acute resolved HBV (right, n = 4) infection. The frequency of HBV pol$_{455}$-specific CD8$^+$ T cells within the total CD8$^+$ T cell population is indicated. Calculated ex vivo frequencies are depicted. **b–d**, Flow cytometric analysis of the activation status (Ki67: endogenous control/chronic HBV, n = 7; acute HBV, n = 5; acute resolved HBV, n = 4; CD38: endogenous control/chronic HBV, n = 5; acute HBV, n = 3; acute resolved HBV, n = 4) (**b**), the memory-associated marker CD127 (endogenous control/chronic HBV, n = 11; acute HBV, n = 7; acute resolved HBV, n = 4) (**c**) and the cytotoxic molecules GZMB and PRF1 as well as the cytolytic regulator NKG7 (endogenous control/chronic HBV, n = 12; acute HBV, n = 7; acute resolved HBV, n = 4) (**d**) in HBV pol$_{455}$-specific CD8$^+$ T cells is shown. Dot plots and statistical graph depicting gating and frequencies of HBV pol$_{455}$-specific CD8$^+$ T cells are displayed. **e**, Dot plots

showing IFNγ-, TNF- and CD107a-producing HBV pol$_{455}$-specific CD8$^+$ T cells (after peptide/HLA-A*02:01 tetramer-enrichment) in response to PMA/ Iono stimulation (left, PMA/Iono stimulation; right, negative control). The percentages of IFNγ-, TNF- and CD107a-producing HBV pol$_{455}$-specific CD8$^+$ T cells were determined (endogenous control/chronic HBV, n = 6; acute HBV, n = 5; acute resolved HBV, n = 6). **f**, Expression levels of PD1 (endogenous control/ chronic HBV, n = 8; acute HBV, n = 7; acute resolved HBV, n = 4) and KLRG1 (endogenous control/chronic HBV, n = 5; acute HBV, n = 3; acute resolved HBV, n = 3) were examined in HBV pol$_{455}$-specific CD8$^+$ T cells. Dot plots and statistical graph depicting gating and frequencies of HBV pol$_{455}$-specific CD8$^+$ T cells are displayed. Each dot represents one HBV pol$_{455}$-specific CD8$^+$ T cell and is color coded as indicated: dark green, endogenous control/chronic HBV; light green, acute HBV; dark gray, acute resolved HBV. Bar charts show the median value with IQR. Statistical analyses were performed by a Kruskal–Wallis test, including Dunn's multiple comparisons test (**a–f**).
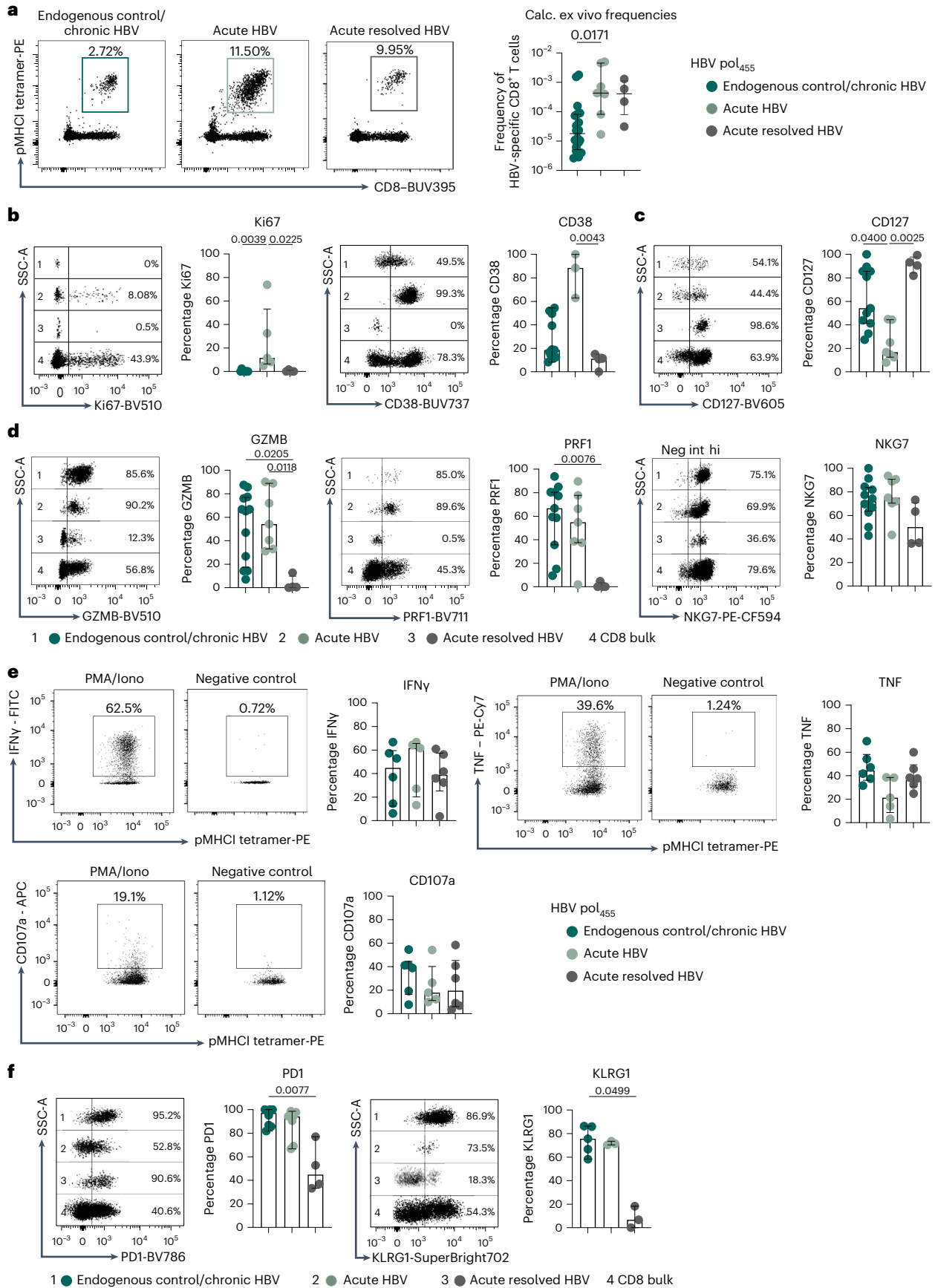
CD127-expressing cells compared to the bona fide virus-specific T cell effector response during the acute phase of HBV infection (Fig. 4c). To compare the functional effector capacity, we first compared the protein expression of cytotoxic molecules in HBV pol$_{455}$-specific CD8$^+$ T cells in acute versus endogenously controlled chronic HBV infection. We did not observe a differential relative expression of the cytotoxic molecules GZMB and PRF1 or the cytolytic regulator NKG7 (Fig. 4d) in contrast to HBV core$_{18}$-specific CD8$^+$ T cells obtained from acute compared to endogenous control/chronic HBV infection (Extended Data Fig. 3a). Next, we tested the ex vivo capacity to produce interferon (IFN)γ, tumor necrosis factor (TNF) or to degranulate in response to PMA/ionomycin stimulation (Fig. 4e). Again, no significant differences were evident comparing HBV pol$_{455}$-specific CD8$^+$ T cells from endogenous control versus acute infection. Additionally, the effector cell markers PD1 and KLRG1 were also not different (Fig. 4f). Hence, while the strength of the HBV pol$_{455}$-specific CD8$^+$ T cell response seems to be attenuated in patients with endogenous control these cells retain the capacity to elicit antiviral effector functions similar to bona fide effector CD8$^+$ T cells. This attenuated HBV pol$_{455}$-specific CD8$^+$ T cell response is clearly different from a bona fide HBV pol$_{455}$-specific memory CD8$^+$ T cell response in patients who spontaneously resolved an acute HBV infection (Extended Data Fig. 3a,b), for example with respect to frequency (Fig. 4a), GZMB, PRF1, KLRG1 and PD1 expression (Fig. 4d,f).

Transcriptional regulation of CD8$^+$ T cell attenuation

To investigate the transcriptional regulation and fate of the attenuated cytotoxic HBV pol$_{455}$-specific CD8$^+$ T cell response in chronic HBV infection, we performed comparative scRNA-seq of HBV pol$_{455}$-specific CD8$^+$ T cells obtained from patients with endogenous control ($n = 3$; 1,921 cells), acute infection ($n = 3$; 1,900 cells) and resolution of acute infection ($n = 2$; 240 cells) using the 10x Genomics platform. Clustering analysis of integrated single-cell transcriptomes of HBV pol$_{455}$-specific CD8$^+$ T cells identified five cell clusters (Fig. 5a). Of note, HBV pol$_{455}$-specific CD8$^+$ T cell cluster identification from scRNA-seq data obtained with the 10x Genomics platform was consistent with the mCEL-seq2 protocol (Extended Data Fig. 4a,b). DEGs comparing these five clusters included *NKG7*, *CX3CR1*, *KLRG1*, *PRF1*, *GZMB*, *PTMA*, *IL7R* and the transcription factors *TBX21*, *RUNX3*, *NR4A2*, *MYBL1*, *ZNF683*, *HMGB1* and *TCF7* (Fig. 5b). More precisely, HBV pol$_{455}$-specific CD8$^+$ T cells from patients with endogenous control could be found in all five clusters with the majority being in cluster 1 that is characterized by cytotoxic effector-like genes (Fig. 5a,b). In contrast, HBV pol$_{455}$-specific CD8$^+$ T cells obtained from patients who were acutely HBV-infected were found in clusters 0, 2, 3 and 4 almost completely omitting cluster 1 (Fig. 5a,b) clearly showing different transcriptional mapping of effector/attenuated cells in acute versus chronic endogenous control HBV infection. After viral resolution, clusters 3 and 4 dominated, probably reflecting T cell memory subsets (Fig. 5a,b). Distinct expression patterns of transcriptional regulators in HBV pol$_{455}$-specific CD8$^+$ T cells from endogenously controlled/chronic, acute and acute resolved phases of HBV infection were confirmed on the protein level (Fig. 5c

and Extended Data Fig. 4c). These differences in ZEB2, T-BET, EOMES, RUNX3 and BLIMP1 expression point toward distinct T cell differentiation programs in acute versus chronic HBV infection irrespective of different VLs (Extended Data Fig. 4d,e). Next, to directly compare effector/effector-like subsets of HBV pol$_{455}$-specific CD8$^+$ T cells obtained from acute-resolving HBV infection versus chronic endogenous control, we compared GZMB $^+$ HBV pol$_{455}$-specific CD8$^+$ T cells as surrogates. Calculated frequencies of GZMB$^+$ HBV pol$_{455}$-specific CD8$^+$ T cells were highest during the acute phase, followed by endogenous control and were only rare in the steady state of acutely resolved HBV infection (Fig. 5d). Furthermore, t-SNE analysis of combined PRF1, NKG7, KLRD1, PD1, CD127, ZEB2, T-BET, EOMES and TOX expression (Fig. 5e and Extended Data Fig. 5a) confirmed topographic separation based on distinct transcription factor patterns. Lower ZEB2, T-BET, EOMES (Fig. 5c) and higher TCF1 expression (Extended Data Fig. 5b) also indicated effector T cell attenuation in endogenous control. In addition to analyzing the transcription factor expression, we also assessed transcription factor activity using SCENIC analysis (Fig. 5f and Extended Data Fig. 5c). Differential transcriptional activity of bona fide effector T cells (cluster 0) in patients who were acutely HBV-infected compared to attenuated T cells (cluster 1) obtained from endogenously controlled/chronically HBV-infected patients further highlighted distinct transcriptional programs (Fig. 5f and Extended Data Fig. 5c). In particular, increased activity of STAT1, TBX21 and IRF9 was detectable in effector T cells (cluster 0), whereas KLF6, FOS, JUN and MYBL1 were highly active in attenuated T cells (cluster 1), highlighting that bona fide effector T cells and attenuated T cells not only differ in transcription factor expression but also in their activity. Taken together, attenuated HBV pol$_{455}$-specific CD8$^+$ T cells exhibit a unique transcriptional program compared to classical effector T cells but are still linked to endogenous viral control in chronic HBV infection.

TGFβ regulates CD8$^+$ T cell attenuation

Next, we set out to address the underlying mechanisms of HBV pol$_{455}$-specific CD8$^+$ T cell attenuation in endogenous control during chronic HBV infection. We focused on TGFβ as it has previously been shown in the mouse model of LCMV infection[33] to lead to dampening of effector T cell differentiation, including downregulation of ZEB2 as observed in our analysis (Fig. 5c). In addition, among the top 30 DEGs, we also detected increased *TGFBR3* expression specifically in attenuated CD8$^+$ T cells targeting HBV pol$_{455}$ in chronic HBV/endogenously controlled infection and not in HBV core$_{18}$-specific CD8$^+$ T cells (Figs. 1b and 2b and Extended Data Fig. 6a). Notably, increased *TGFBR3* and *TGFBR1* expression levels were also evident comparing attenuated with bona fide effector or memory HBV pol$_{455}$-specific CD8$^+$ T cells (Fig. 6a) and in a previously published dataset[34] of GZMB$^+$CD8$^+$ T cells (Extended Data Fig. 6b) sampled from the liver of chronically HBV-infected patients with endogenous control by fine-needle aspiration (FNA). These observations support the hypothesis of increased TGFβ responsiveness in CD8$^+$ T cell attenuation. In line with this, we observed a significant enrichment of TGFβ and not IL-10 signaling pathway genes in

Fig. 5 | Unique transcriptional regulation of attenuated HBV pol$_{455}$-specific CD8$^+$ T cells. a, Cluster analysis via Seurat and Harmony algorithm applied to single-cell transcriptomes of HBV pol$_{455}$-specific CD8$^+$ T cells obtained from endogenous control/chronic HBV ($n = 3$), acute HBV ($n = 3$) and acute resolved HBV ($n = 2$) infection using 10x Genomics platform. Each dot corresponds to one individual cell. Five clusters (C0–4) were identified and color coded according to disease phases. **b**, Bubble plot of DEGs among C0–4 is displayed. Scaled expression is depicted. **c**, Flow cytometric analysis of transcription factors linked to effector cell differentiation (ZEB2, T-BET, EOMES) was performed in HBV pol$_{455}$-specific CD8$^+$ T cells (endogenous control/chronic HBV, $n = 13$; acute HBV, $n = 7$; acute resolved HBV, $n = 4$). Histograms and statistical graph depicting gating and frequencies of HBV pol$_{455}$-specific CD8$^+$ T cells are displayed. **d**, The calculated frequencies of GZMB$^+$ HBV pol$_{455}$-specific CD8$^+$ T cells within the total CD8$^+$ T cell population are depicted (endogenous control/chronic HBV, $n = 12$; acute HBV, $n = 7$; acute resolved HBV, $n = 4$). **e**, t-SNE representation of concatenated flow cytometry data gated on GZMB$^+$ HBV pol$_{455}$-specific CD8$^+$ T cells is illustrated. Scaled expression (blue, low; red, high) is depicted. **f**, Binary regulon activity based on SCENIC analysis is depicted in violin plots (box center line, median; box limits, upper and lower quartiles; box whiskers, interquartile range (IQR)) comparing C0 and C1 (endogenous control/chronic HBV, $n = 3$; acute HBV, $n = 3$; acute resolved HBV, $n = 2$). Each dot represents one HBV pol$_{455}$-specific CD8$^+$ T cell and is color coded as indicated: dark green, endogenous control/chronic HBV; light green, acute HBV; dark gray, acute resolved HBV. Bar charts show the median value with IQR. Statistical significance was assessed by a Kruskal–Wallis test, including Dunn's multiple comparisons test (**c**,**d**) and two-tailed Mann–Whitney test (**f**).

HBV pol$_{455}$-specific CD8$^+$ T cells in endogenous control/chronic versus acute and acute resolved HBV infection (Fig. 6b and Extended Data Fig. 6c). These results argue against a general responsiveness of attenuated HBV pol$_{455}$-specific CD8$^+$ T cells toward suppressive cytokines and rather support a distinct role for TGFβ signaling. To further determine the direct impact of TGFβ signaling on the effector T cell program in the context of HBV infection, we performed peptide-specific expansion of HBV pol$_{455}$-specific CD8$^+$ T cells in the presence or absence of the TGFβ RI kinase inhibitor II CAS 446859-33-2 (Fig. 6c). Blocking of TGFβ signaling led to an increase in the expression of ZEB2, T-BET, EOMES, GZMB
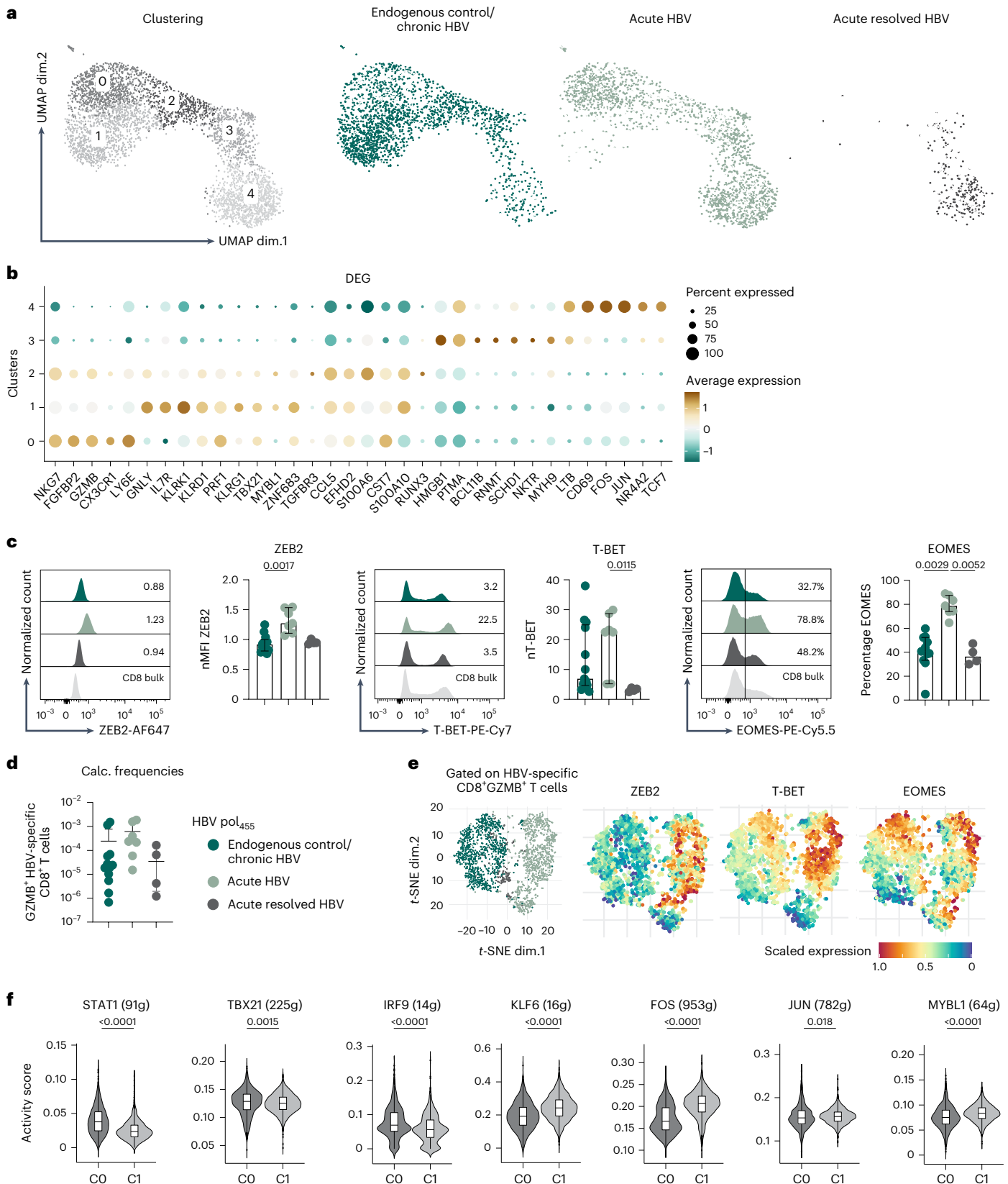
and PRF1 in HBV pol$_{455}$-specific CD8$^+$ T cells of patients with endogenous control, whereas ZEB2 and T-BET expression remained stable in HBV pol$_{455}$-specific CD8$^+$ T cells obtained from patients acutely infected with HBV (Fig. 6d and Extended Data Fig. 6d,e). Accordingly, inhibition of TGFβ signaling resulted in an increase of HBV pol$_{455}$-specific IFNγ and TNF production of CD8$^+$ T cells in all but one tested patient with endogenous control, along with a significant boost of IFNγ and TNF co-producing cells in all tested patients and an elevated HBV pol$_{455}$-specific degranulation (indicated by CD107a expression) of CD8$^+$ T cells in three out of six tested patients (Extended Data Fig. 7). These data indicate an augmented function of HBV pol$_{455}$-specific CD8$^+$ T cells after TGFβ inhibition. Moreover, we also detected higher TGFβ concentrations in the plasma of patients with endogenous control/chronic ($n = 21$) compared to acute ($n = 7$) and acute resolved ($n = 6$) HBV infection of whom we have also analyzed the HBV pol$_{455}$-specific CD8$^+$ T cell responses previously (Extended Data Fig. 6f).

Next, to test which factor may also impact on HBV pol$_{455}$-specific CD8$^+$ T cell attenuation and may be used to boost or even release these cells, we conducted GSEA of the IL-2, IL-12 and IFNα signaling pathways and performed peptide-specific expansion of HBV pol$_{455}$-specific CD8$^+$ T cells this time in the presence of either IL-12 or IFNα. Based on expression of cytokine signaling pathway genes, we observed an enrichment of the IL-12 pathway in attenuated HBV pol$_{455}$-specific CD8$^+$ T cells versus bona fide effector and memory subsets, but a decrease in IFNα and IL-2 pathway gene expression compared to acute and acutely resolved HBV infection (Extended Data Fig. 8a). Stimulation with IL-12 resulted in increased expression of T-BET, EOMES and perforin (Fig. 6e,f and Extended Data Fig. 8b), whereas stimulation with IFNα only led to an augmented T-BET expression (Fig. 6e,g and Extended Data Fig. 8c). Given these different effects of cytokine interventions on the T cell program, we next wondered which treatment redirected/boosted attenuated HBV pol$_{455}$-specific CD8$^+$ T cells most similar toward bona fide effector cells detectable during acute HBV. Dimensional reduction analyses by t-SNE and multidimensional scaling (MDS) revealed that TGFβ blockade directed attenuated HBV pol$_{455}$-specific CD8$^+$ T cells most efficiently toward bona fide effector cells accompanied by the largest boost in expansion (Fig. 6h and Extended Data Fig. 8d). Hence, while IL-12 and IFNα can partly redirect attenuated HBV pol$_{455}$-specific CD8$^+$ T cells, TGFβ signaling seems to be a key regulator of HBV-specific CD8$^+$ T cell attenuation present in the endogenous control phase of chronic HBV infection.

Discussion

Here, we report the identification of an attenuated cytotoxic HBV-specific CD8$^+$ T cell population that is present during chronic human viral infection and that is linked to endogenous viral control. Attenuated HBV-specific CD8$^+$ T cells exhibited similar expression of effector cell markers such as PD1, KLRG1, CX3CR1, NKG7 and of cytotoxic molecules and cytokine production capacities when compared to effector HBV-specific CD8$^+$ T cells obtained from acute-resolving infection underlining their potent effector functions; however, concomitantly, they displayed higher levels of markers for T cell maintenance, such as CD127 and TCF1 and lower expression of transcriptional regulators of the cytotoxic effector T cell program, such as EOMES and ZEB2 (refs. 28,35,36), indicating an adapted attenuated T cell differentiation program in chronic infection. Still, despite the presence of chronic infection, the attenuated HBV-specific CD8$^+$ T cell population does not show typical features of T cell exhaustion. Indeed, scRNA-seq analysis revealed unique clusters of cells that did not overlap with the molecular core signature underlying exhausted CD8$^+$ T$_{EX}$ cells present during chronic human HCV[25] and LCMV[17] infection including the STAT5-dependent effector-like T$_{EX}$ cells[28,29,37]. Accordingly, they followed a trajectory that separates from effector and exhausted cells and are clearly distinct from a memory T cell response supporting a unique program and fate of this cell subset in chronic HBV infection.

Key determinants of T cell tuning, adaptation and, thus, fate are antigen recognition dynamics (for example, dose and duration) as well as co-stimulation and cytokine milieu[38–44]. Attenuated HBV-specific CD8$^+$ T cells were mainly targeting the HBV polymerase antigen and hardly any HBV core antigen, highlighting the impact of specific antigen recognition in the induction of the attenuated T cell fate. Of note, HBV polymerase and HBV core exhibit a mosaic pattern of antigen presentation in the infected liver with lower quantities of HBV polymerase compared to core[45]. In addition to antigen recognition, T cell attenuation is also shaped by a TGFβ cytokine milieu, with ZEB2 being a relevant rheostat. In particular, we observed significantly higher TGFβ plasma levels in patients who were chronically HBV-infected (in line with findings by others[46]) and an increase in the expression of ZEB2 in HBV pol$_{455}$-specific CD8$^+$ T cells after blockade of TGFβ. This is in line with previous findings in the LCMV mouse model showing that ZEB2 is selectively inhibited by TGFβ[33] and that TGFβ signaling as well as ZEB2 deletion suppress the effector-associated program of CD8$^+$ T cells[47]. Notably, HBV-specific T cell attenuation could only be partly overcome by co-stimulatory cytokine stimulations, including IL-2, IL-12 and type I IFNs with no effect on ZEB2 expression. Combined, these results support an important role of antigen recognition and TGFβ signaling linked to ZEB2 expression in HBV-specific CD8$^+$ T cell attenuation in chronic infection. Whether TGFβ inhibition represents a feasible treatment option to boost the HBV-specific CD8$^+$ T cell response in patients chronically infected with HBV requires further investigation. The clinical application of TGFβ inhibition remains challenging due to pleiotropic effects and adverse events. Still, therapeutic potential of TGFβ inhibition has been and is currently tested in several clinical trials[48], especially in the context of cancer treatment. For example, combination with checkpoint blockade inhibition revealed an enhanced increase in virus-specific CD8$^+$ T cells in HPV-related cancer associated with an objective treatment response[48]. Hence, TGFβ inhibitors seem to be feasible and promising in clinical application of virus-associated diseases.

Fig. 6 | TGFβ signaling is linked to HBV-specific CD8$^+$ T cell attenuation.
a, Bubble plot showing TGFβ receptor gene expression in HBV pol$_{455}$-specific CD8$^+$ T cells of endogenous control/chronic HBV ($n = 3$), acute HBV ($n = 3$) and acute resolved HBV infection ($n = 2$). Scaled expression levels are color coded (blue, low; brown, high). **b**, KEGG analysis of the TGFβ signaling pathway in HBV pol$_{455}$-specific CD8$^+$ T cells of endogenous control/chronic HBV, acute HBV and acute resolved HBV infection. The aggregated transcript counts are mapped in violin plots. **c**, Experimental workflow of peptide-specific in vitro expansion of CD8$^+$ T cells is illustrated. TGFβ signaling was blocked by adding TGF-β RI kinase inhibitor II CAS 446859-33-2 into the cell culture. **d**, Dot plots showing ZEB2, EOMES and GZMB expression of HBV pol$_{455}$-specific CD8$^+$ T cells after 14 days of in vitro culture with (left) and without TGF-β RI kinase inhibitor II (right) (endogenous control/chronic HBV, $n = 6$). Statistical graph depicting frequencies of ZEB2$^+$, T-BET$^+$, EOMES$^+$ or GZMB$^+$ HBV pol$_{455}$-specific CD8$^+$ T cells are displayed. **e**, Experimental workflow of peptide-specific in vitro expansion of CD8$^+$ T cells treated with IL-12 or IFNα is illustrated. **f,g**, ZEB2, T-BET, EOMES and GZMB expression of HBV pol$_{455}$-specific CD8$^+$ T cells after 14 days of in vitro culture with IL-12 (endogenous control/chronic HBV, $n = 7$) (**f**) or IFNα treatment (**g**) (endogenous control/chronic HBV, $n = 8$) or without any treatment is shown. **h**, t-SNE (left) and MDS (right) representations of concatenated flow cytometry data gated on HBV pol$_{455}$-specific CD8$^+$ T cells of acute HBV ($n = 7$) and endogenous control/chronic HBV infection (ex vivo, $n = 13$) or the later one after IL-2 treatment ($n = 10$), after blocking of TGFβ signaling ($n = 6$) or treatment with IL-12 ($n = 7$) or IFNα ($n = 8$), is illustrated. Each dot represents one of the respective HBV pol$_{455}$-specific CD8$^+$ T cell responses with color coding as indicated: dark green, endogenous control/chronic HBV; light green, acute HBV. Statistical analyses were performed via Kruskal–Wallis test, including Dunn's multiple comparisons test (**b**) and two-tailed Wilcoxon matched-pairs signed-rank test (**d,f,g**).

The emergence of attenuated HBV-specific CD8^{+} T cells was strictly associated with the so termed HBeAg− chronic HBV infection phase of chronic HBV infection. Of note, testing of the HBeAg^{+} chronic HBV infection and HBeAg[+] hepatitis B phases warrant further investigations as we restricted our analyses to the HBeAg− disease phases of chronic

HBV infection to cover the majority of patients in advanced countries. The clinical phase of HBeAg− chronic HBV infection is characterized by low or even hardly detectable VL and normal levels of transaminases reflecting endogenous viral control and limited immunopathology. This observation proposes a clear link of the T cell program and
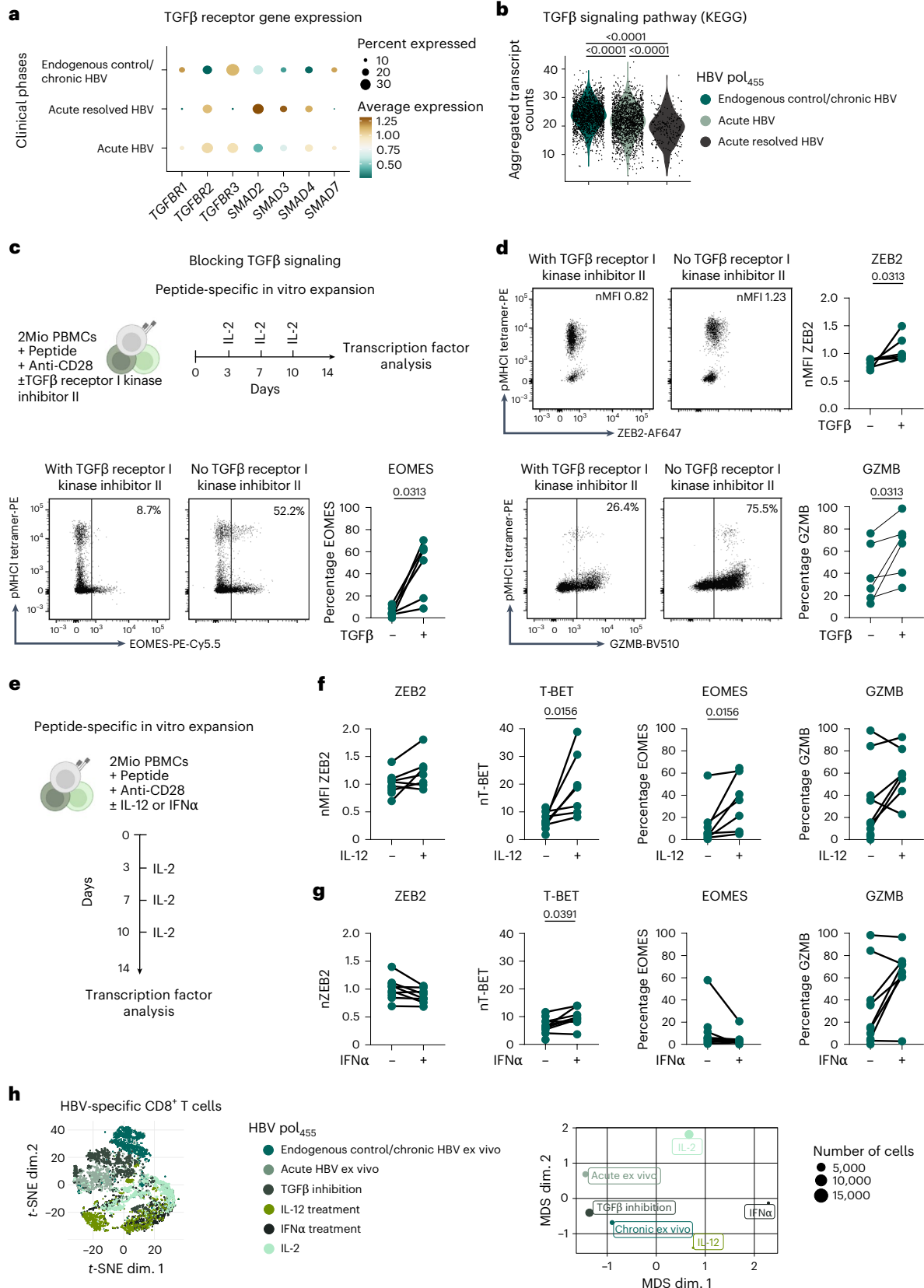
differentiation to the clinical course in chronic HBV infection. Furthermore, it reveals that HBV-specific CD8+ T cells are not 'nonfunctional' but rather adapted during chronic infection strongly highlighting the important antiviral efficiency of HBV-specific CD8+ T cells also during the chronic phase of HBV infection. Subsequently, CD8+ T cells involving viral containment come along with reduced HBV-triggered immunopathology. Functional adaptation within the HBV-specific CD8+ T cell attenuation program also comprises the maintenance of these cells in the context of persistent antigen stimulation guided by TCF1 and CD127. This ensures ongoing HBV-specific CD8+ T cell surveillance by attenuated subsets in chronic HBV infection, contributing to endogenous control. Functional HBV-specific T cells have recently been reported as candidate immunological biomarkers for safe therapy discontinuation in patients with chronic HBV[49,50] and in spontaneously controlling patients with HIV infection[51] underpinning the translational value of this concept with respect to therapeutic approaches and beyond chronic HBV infection. In our study, we have not confirmed the presence of attenuated HBV-specific CD8+ T cells at the site of infection, the liver; however, circulating CD8+ T cells adhere and/or infiltrate the HBV-infected liver[52], thereby comprising an important part of the T cell-mediated surveillance in HBV infection. Moreover, they represent the T cell compartment that can be clinically monitored. All in all, our results unravel a clinically relevant new layer of functional adaptation of antiviral CD8+ T cell immunity in chronic HBV infection next to the previously reported phenotypic and functional heterogeneity that is shaped by the underlying viral infection (HBV versus HCV), the targeted antigen (core versus polymerase)[18,19], ongoing replication[21], duration of infection, age or the tissue distribution[45]. By this, we showed the existence of a specific T cell programming beyond T cell exhaustion in humans that has a clinically relevant role by the potential to contribute to viral containment during chronic infection.

Online content

Any methods, additional references, Nature Portfolio reporting summaries, source data, extended data, supplementary information, acknowledgements, peer review information; details of author contributions and competing interests; and statements of data and code availability are available at https://doi.org/10.1038/s41590-024-01928-4.

References

1. World Health Organization. Hepatitis B. https://www.who.int/news-room/fact-sheets/detail/hepatitis-b (2024).
2. EASL. 2017 Clinical Practice Guidelines on the management of hepatitis B virus infection. *J. Hepatol.* **67**, 370–398 (2017).
3. Thimme, R. et al. CD8(+) T cells mediate viral clearance and disease pathogenesis during acute hepatitis B virus infection. *J. Virol.* **77**, 68–76 (2003).
4. Maini, M. K. et al. The role of virus-specific CD8(+) cells in liver damage and viral control during persistent hepatitis B virus infection. *J. Exp. Med.* **191**, 1269–1280 (2000).
5. Webster, G. J. et al. Longitudinal analysis of CD8+ T cells specific for structural and nonstructural hepatitis B virus proteins in patients with chronic hepatitis B: implications for immunotherapy. *J. Virol.* **78**, 5707–5719 (2004).
6. Boni, C. et al. Characterization of hepatitis B virus (HBV)-specific T-cell dysfunction in chronic HBV infection. *J. Virol.* **81**, 4215–4225 (2007).
7. Das, A. et al. Functional skewing of the global CD8 T cell population in chronic hepatitis B virus infection. *J. Exp. Med.* **205**, 2111–2124 (2008).
8. Kurktschiev, P. D. et al. Dysfunctional CD8+ T cells in hepatitis B and C are characterized by a lack of antigen-specific T-bet induction. *J. Exp. Med.* **211**, 2047–2059 (2014).
9. Schurich, A. et al. Distinct metabolic requirements of exhausted and functional virus-specific CD8 T cells in the same host. *Cell Rep.* **16**, 1243–1252 (2016).
10. Fisicaro, P. et al. Targeting mitochondrial dysfunction can restore antiviral activity of exhausted HBV-specific CD8 T cells in chronic hepatitis B. *Nat. Med.* **23**, 327–336 (2017).
11. Heim, K. et al. TOX defines the degree of CD8+ T cell dysfunction in distinct phases of chronic HBV infection. *Gut* **70**, 1550–1560 (2020).
12. Wherry, E. J. & Kurachi, M. Molecular and cellular insights into T cell exhaustion. *Nat. Rev. Immunol.* **15**, 486–499 (2015).
13. McLane, L. M., Abdel-Hakeem, M. S. & Wherry, E. J. CD8 T cell exhaustion during chronic viral infection and cancer. *Annu. Rev. Immunol.* **37**, 457–495 (2019).
14. Bengsch, B. et al. Coexpression of PD-1, 2B4, CD160 and KLRG1 on exhausted HCV-specific CD8+ T cells is linked to antigen recognition and T cell differentiation. *PLoS Pathog.* **6**, e1000947 (2010).
15. Alfei, F. et al. TOX reinforces the phenotype and longevity of exhausted T cells in chronic viral infection. *Nature* **571**, 265–269 (2019).
16. Blackburn, S. D., Shin, H., Freeman, G. J. & Wherry, E. J. Selective expansion of a subset of exhausted CD8 T cells by αPD-L1 blockade. *PNAS* **105**, 15016–15021 (2008).
17. Utzschneider, D. T. et al. T cell factor 1-expressing memory-like CD8(+) T cells sustain the immune response to chronic viral infections. *Immunity* **45**, 415–427 (2016).
18. Schuch, A. et al. Phenotypic and functional differences of HBV core-specific versus HBV polymerase-specific CD8+ T cells in chronically HBV-infected patients with low viral load. *Gut* **68**, 905–915 (2019).
19. Hoogeveen, R. C. et al. Phenotype and function of HBV-specific T cells is determined by the targeted epitope in addition to the stage of infection. *Gut* **68**, 893–904 (2019).
20. Winkler, F. et al. Enolase represents a metabolic checkpoint controlling the differential exhaustion programmes of hepatitis virus-specific CD8(+) T cells. *Gut* **72**, 1971–1984 (2023).
21. Cheng, Y. et al. Multifactorial heterogeneity of virus-specific T cells and association with the progression of human chronic hepatitis B infection. *Science Immunol.* **4**, eaau6905 (2019).
22. Aliabadi, E. et al. Impact of HBsAg and HBcrAg levels on phenotype and function of HBV-specific T cells in patients with chronic hepatitis B virus infection. *Gut* **71**, 2300–2312 (2022).
23. Bertoletti, A. & Ferrari, C. Adaptive immunity in HBV infection. *J. Hepatol.* **64**, S71–s83 (2016).
24. Herman, J. S., Sagar & Grün, D. FateID infers cell fate bias in multipotent progenitors from single-cell RNA-seq data. *Nat. Methods* **15**, 379–386 (2018).
25. Hensel, N. et al. Memory-like HCV-specific CD8(+) T cells retain a molecular scar after cure of chronic HCV infection. *Nat. Immunol.* **22**, 229–239 (2021).
26. Hao, Y. et al. Integrated analysis of multimodal single-cell data. *Cell* **184**, 3573–3587.e3529 (2021).
27. Korsunsky, I. et al. Fast, sensitive and accurate integration of single-cell data with Harmony. *Nat. Methods* **16**, 1289–1296 (2019).
28. Giles, J. R. et al. Shared and distinct biological circuits in effector, memory and exhausted CD8(+) T cells revealed by temporal single-cell transcriptomics and epigenetics. *Nat. Immunol.* **23**, 1600–1613 (2022).
29. Beltra, J. C. et al. Stat5 opposes the transcription factor Tox and rewires exhausted CD8(+) T cells toward durable effector-like states during chronic antigen exposure. *Immunity* **56**, 2699–2718. e2611 (2023).
30. Giles, J. R. et al. Human epigenetic and transcriptional T cell differentiation atlas for identifying functional T cell-specific enhancers. *Immunity* **55**, 557–574.e557 (2022).

31. Haghverdi, L., Büttner, M., Wolf, F. A., Buettner, F. & Theis, F. J. Diffusion pseudotime robustly reconstructs lineage branching. *Nat. Methods* **13**, 845–848 (2016).

32. Aibar, S. et al. SCENIC: single-cell regulatory network inference and clustering. *Nat. Methods* **14**, 1083–1086 (2017).

33. Guan, T. et al. ZEB1, ZEB2, and the miR-200 family form a counterregulatory network to regulate CD8(+) T cell fates. *J. Exp. Med.* **215**, 1153–1168 (2018).

34. Genshaft, A. S. et al. Single-cell RNA sequencing of liver fine-needle aspirates captures immune diversity in the blood and liver in chronic hepatitis B patients. *Hepatology* **78**, 1525–1541 (2023).

35. Dominguez, C. X. et al. The transcription factors ZEB2 and T-bet cooperate to program cytotoxic T cell terminal differentiation in response to LCMV viral infection. *J. Exp. Med.* **212**, 2041–2056 (2015).

36. Omilusik, K. D. et al. Transcriptional repressor ZEB2 promotes terminal differentiation of CD8⁺ effector and memory T cell populations during infection. *J.f Exp. Med.* **212**, 2027–2039 (2015).

37. Daniel, B. et al. Divergent clonal differentiation trajectories of T cell exhaustion. *Nat. Immunol.* **23**, 1614–1627 (2022).

38. Iezzi, G., Karjalainen, K. & Lanzavecchia, A. The duration of antigenic stimulation determines the fate of naive and effector T cells. *Immunity* **8**, 89–95 (1998).

39. Shedlock, D. J. & Shen, H. Requirement for CD4 T cell help in generating functional CD8 T cell memory. *Science* **300**, 337–339 (2003).

40. Kolumam, G. A., Thomas, S., Thompson, L. J., Sprent, J. & Murali-Krishna, K. Type I interferons act directly on CD8 T cells to allow clonal expansion and memory formation in response to viral infection. *J. Exp. Med.* **202**, 637–650 (2005).

41. Mescher, M. F. et al. Signals required for programming effector and memory development by CD8⁺ T cells. *Immunol. Rev.* **211**, 81–92 (2006).

42. Williams, M. A., Tyznik, A. J. & Bevan, M. J. Interleukin-2 signals during priming are required for secondary expansion of CD8⁺ memory T cells. *Nature* **441**, 890–893 (2006).

43. Joshi, N. S. et al. Inflammation directs memory precursor and short-lived effector CD8(+) T cell fates via the graded expression of T-bet transcription factor. *Immunity* **27**, 281–295 (2007).

44. Ruby, C. E., Redmond, W. L., Haley, D. & Weinberg, A. D. Anti-OX40 stimulation in vivo enhances CD8⁺ memory T cell survival and significantly increases recall responses. *Eur. J. Immunol.* **37**, 157–166 (2007).

45. Khakpoor, A. et al. Spatiotemporal differences in presentation of CD8 T cell epitopes during hepatitis B virus infection. *J. Virol.* **93**, e01457–18 (2019).

46. Wiegand, S. B. et al. Soluble immune markers in the different phases of chronic hepatitis B virus infection. *Sci. Rep.* **9**, 14118 (2019).

47. Dahmani, A. & Delisle, J. S. TGF-β in T cell biology: implications for cancer immunotherapy. *Cancers* **10**, 194 (2018).

48. Metropulos, A. E. & Munshi, H. G. & Principe, D.R. The difficulty in translating the preclinical success of combined TGFβ and immune checkpoint inhibition to clinical trial. *eBioMedicine* **86**, 104380 (2022).

49. Rivino, L. et al. Hepatitis B virus-specific T cells associate with viral control upon nucleos(t)ide-analogue therapy discontinuation. *J. Clin. Investig.* **128**, 668–681 (2018).

50. Tian, Y., James Ou, J. H., Hepatitis, B. & Virus-Specific, T. Cells as a biomarker for discontinuation of nucleos(t)ide analogue therapy for chronic hepatitis B. *Hepatology* **69**, 1342–1344 (2019).

51. Collins, D. R., Gaiha, G. D. & Walker, B. D. CD8(+) T cells in HIV control, cure and prevention. *Nat. Rev. Immunol.* **20**, 471–482 (2020).

52. Pallett, L. J. & Maini, M. K. Liver-resident memory T cells: life in lockdown. *Semin. Immunopathol.* https://doi.org/10.1007/s00281-022-00932-w (2022).

¹Department of Medicine II, Medical Center – University of Freiburg, Freiburg, Germany. ²Faculty of Medicine, University of Freiburg, Freiburg, Germany. ³Division of Infection and Immunity, Cardiff University School of Medicine, University Hospital of Wales, Cardiff, UK. ⁴Systems Immunity Research Institute, Cardiff University School of Medicine, University Hospital of Wales, Cardiff, UK. ⁵Institute for Transfusion Medicine and Gene Therapy, University Medical Center, University of Freiburg, Freiburg, Germany. ⁶Department of Gastroenterology, Hepatology, Infectious Diseases and Endocrinology, Hannover Medical School, Hannover, Germany. ⁷German Centre for Infection Research (DZIF), partner site Hannover-Braunschweig, Braunschweig, Germany. ⁸Centre for Individualised Infection Medicine (CiiM), Hannover, Germany. ⁹Cluster of Excellence Resolving Infection Susceptibility (RESIST; EXC), Hannover Medical School, Hannover, Germany. ¹⁰Institute of Molecular Immunology, School of Medicine, Technical University of Munich (TUM), Munich, Germany. ¹¹German Center for Infection Research, Munich, Germany. ¹²Institute of Molecular Immunology, School of Life Science, TUM, Munich, Germany. ¹³Signaling Research Centres BIOSS and CIBSS, University of Freiburg, Freiburg, Germany. ¹⁴These authors contributed equally: Kathrin Heim, Sagar. ¹⁵These authors jointly supervised this work: Robert Thimme, Maike Hofmann. ✉e-mail: robert.thimme@uniklinik-freiburg.de; maike.hofmann@uniklinik-freiburg.de

Methods

Study cohort

Blood samples of participants with viral hepatitis were recruited at the Department of Medicine II of the University Hospital Freiburg, Germany and at the Department of Gastroenterology, Hepatology and Endocrinology and at Hannover Medical School, Hannover, Germany. In total, 80 HLA-A*02:01-positive individuals and 14 HLA-B*35:01-positive individuals with chronic HBV infection were included in this study. Individuals were classified into different clinical phases of chronic HBV infection according to EASL guidelines that consider the presence of HBeAg, HBV DNA levels, transaminase levels (alanine transaminase (ALT) and aspartate transferase (AST)) and the presence or absence of liver inflammation[2]. Throughout the entire study, the HBeAg− cHBV infection phase is referred to as endogenous control/chronic HBV. The HBeAg− CHB phase is specified as high VL/chronic HBV and individuals within the HBeAg− CHB phase and under nucleos(t)ide analogs (NUC) treatment are indicated as NUC control/chronic HBV. In addition, eight HLA-A*02:01-positive individuals with acute HBV infection as well as 11 HLA-A*02:01-positive individuals who resolved an acute HBV infection were enrolled in this study. Characteristics of included individuals are summarized in Supplementary Tables 1–6. HBeAg, serum HBV DNA and AST/ALT values were determined as part of the clinical diagnostics at the University Hospital Freiburg, Germany. Confirmation of HLA-A*02:01 was performed by four-digit HLA-typing by next-generation sequencing on an MiSeq system using commercially available primers (GenDx). Due to limitations of sample material per patient we were not able to perform all analyses with cells from all patients. Detailed information about the inclusion of the patients in the different analyses are given in the Source data.

Ethics

Written informed consent was obtained from all participants before blood donation. Consent covers data publication after anonymization. The study was conducted according to federal guidelines, local ethics committee regulations of Albert-Ludwigs-Universität, Freiburg, Germany (no. 474/14, 383/19, 384/18), Hannover Medical School, Hannover, Germany (no. 3374-2016) and the Declaration of Helsinki (1975).

PBMC isolation

Venous blood samples were collected in EDTA-anticoagulated tubes. Peripheral blood mononuclear cells (PBMCs) were isolated by density gradient centrifugation using lymphocyte separation medium (PAN Biotech) and stored at −80 °C until usage. Frozen PBMCs were thawed in complete medium (RPMI 1640 supplemented with 10% fetal calf serum, 1% penicillin/streptomycin and 1.5% 1 M HEPES buffer (all additives from Thermo Scientific)) containing 50 U ml^{-1} Benzonase (Sigma).

Peptides and tetramers

Peptides of immunodominant HBV-derived epitopes (HLA-A*02:01/ HBV core$_{18}$, FLPSDFFPSV; HLA-A*02:01/HBV pol$_{455}$, GLSRYVARL; HLA-B*35:01/HBV pol$_{173}$, SPYSWEQEL) were synthesized with standard Fmoc chemistry and a purity of >70% from Genaxxon. HLA class I epitope-specific tetramers were generated through conjugation of biotinylated peptide/HLA class I monomers with PE-conjugated streptavidin (Agilent) at a peptide/HLA I: streptavidin molar ratio of 5:1. Of note, targeted epitopes of HBV-specific CD8$^+$ T cells were previously analyzed for viral sequence mutations. T cell responses of patients harboring viral sequence mutations in the targeted epitope were excluded.

HBV viral sequencing

Viral DNA was extracted from 0.75–1.0 ml patient's plasma at the used bleed date or latest available HBV DNA-positive time point using QIAamp UltraSens technology (QIAGEN) according to the manufacturer's protocol. A two-step nested PCR approach was used to amplify HBV DNA fragments for viral sequence analyses of HBV epitopes. The following specific primers were used: HBV core$_{18}$/13F1 (5′-CACCTCTGCCTAATCATCTC-3′), HBV core$_{18}$/499R1 (5′-CCGGAAGTGTT GATAAGATAGG-3′), HBV core$_{18}$/46F2 (5′-ACTGT TCAAGCCTCCAAGCTG-3′), HBV core$_{18/455}$R2 (5′-GAGGAGTGCGA-ATCCACACTC-3′), HBV pol$_{455}$/ 1384F1 (5′-ACCAAACT CTGCARGAT-CCCAG-3′), HBV pol$_{455}$/2467R1 (5′-TGGTGGCTCCAGTTCAGGAAC-3′), HBV pol$_{455}$/1430F2 (5′-TGGTGGCTCCAGTTCAGGAAC-3′), HBV pol$_{455}$/ 2324R2 (5′-ATCAATAGG CCTGTTAACAGGAAG-3′), HBV pol$_{173}$/454F1 (5′-GGAGTGTGGATTCGCACTCC-3′), HBV pol$_{173}$/ 3146R1 (5′-CCAA-TTTATGCCTACAGCCTC-3′), HBV pol$_{173}$/484F2 (5′-AGACCACCAA ATGCCCCTATC-3′) and HBV pol$_{173}$/3143R2 (5′-CAATTTATGCCTAC-AGCCTCCTA-3′). Purified PCR products were sequenced via Sanger sequencing (Eurofins). Sequences and chromatograms were evaluated with the program Geneious (Biomatters), allowing comparison with wild-type reference sequences (NCBI accession codes: genotype A X02763, genotype D X02496 and genotype E X75657).

Magnetic bead-based enrichment of HBV epitope-specific CD8$^+$ T cells

Enrichment of HBV epitope-specific CD8$^+$ T cells was performed. In brief, 1×10^7 to 2×10^7 PBMCs were labeled for 30 min with PE-coupled peptide-loaded HLA class I tetramers. Enrichment was then carried out with anti-PE microbeads using magnetic-activated cell sorting technology (Miltenyi Biotec) according to the manufacturer's instructions. Subsequently, enriched HBV epitope-specific CD8$^+$ T cells were used for multiparametric flow cytometric analysis. Ex vivo frequency of HBV epitope-specific CD8$^+$ T cells were calculated as follows. First, the number of total CD8$^+$ T cells within the analyzed sample was determined by multiplying the (counted) total number of PBMCs in the pre-enriched sample with the frequency of single, live, non-dump CD8$^+$ T cells in the pre-enriched sample. The absolute number of virus-specific CD8$^+$ T cells was the number of HBV epitope-specific CD8$^+$ T cells within the single, live, non-dump CD8$^+$ T cell gate present in the enriched fraction. The frequency of circulating HBV epitope-specific CD8$^+$ T cells was defined as the absolute number of HBV epitope-specific CD8$^+$ T cells/ absolute number of CD8$^+$ T cells.

Ex vivo functional CD8$^+$ T cell capacity assay

After magnetic bead-based enrichment of HBV pol$_{455}$-specific CD8$^+$ T cells, enriched samples were stimulated with PMA (50 ng ml^{-1}) and ionomycin (1 µg ml^{-1}) (all Sigma) in the presence of anti-CD107a (H4A3, 1:100, cat. 560664, BD Bioscience) to detect the degranulation surrogate CD107a. To assess the intracellular cytokine production, brefeldin A (GolgiPlug, 0.5 µl ml^{-1}) and monensin (GolgiStop, 0.5 µl ml^{-1}) (all BD Biosciences) were added after 1 h. After an additional 3 h of incubation, surface and intracellular staining were performed. One-third of the enriched fractions were used as unstimulated controls for background subtraction. Of note, the low frequency of HBV-specific CD8$^+$ T cells hinders testing of the functional activity in response to peptide stimulation; however, stimulation with PMA/ ionomycin enables testing of the functional capacity of CD8$^+$ T cells, bypassing TCR signaling and thus allowing previous peptide-loaded HLA class I-based enrichment of HBV-specific CD8$^+$ T cells to increase the sensitivity.

TGFβ signaling blockade assay

Approximately 2×10^6 PBMCs were stimulated with HBV pol$_{455}$-specific peptide (GLSRYVARL, 10 µg ml^{-1}) and anti-CD28 monoclonal antibody (0.5 µg ml^{-1}, BD Bioscience) and expanded at 37 °C for 14 days in complete culture medium containing rIL-2 (20 IU ml^{-1}, STEMCELL Technologies). Then, 50 ng ml^{-1} TGF-β RI kinase inhibitor II CAS 446859-33-2 (Sigma-Aldrich), was added every 3–4 days. Expanded HBV pol$_{455}$-specific CD8$^+$ T cells without inhibition of TGF-β RI kinase were used as control.

Treatment of HBV pol$_{455}$-specific CD8$^+$ T cells with IL-12 or IFNα

Approximately $1-2 \times 10^6$ PBMCs were stimulated with HBV pol$_{455}$-specific peptide (10 µg ml^{-1}) and anti-CD28 monoclonal antibody (0.5 µg ml^{-1}, BD Bioscience) and expanded at 37 °C for 14 days in complete culture medium containing rIL-2 (20 IU ml^{-1}, STEMCELL Technologies). Then, 10 ng ml^{-1} rIL-12 (Sigma) or 1,000 U ml^{-1} IFNα (STEMCELL Technologies) were added every 3–4 days to the respective culture. Expanded HBV pol$_{455}$-specific CD8$^+$ T cells without any treatment were used as control.

TGFβ ELISA

Human TGFβ1 ELISA (Invitrogen) was performed according to the manufacturer's protocol. In brief, standards and plasma samples or supernatant of 4 h PMA (50 ng ml^{-1}) and ionomycin (1 µg ml^{-1}) (all Sigma)-stimulated enriched HBV pol$_{455}$-specific CD8$^+$ T cells were pipetted into preassigned wells. After 2 h of incubation and washing, a biotin-conjugated anti-human TGFβ1 antibody was added and bound to human TGFβ1 captured by the first antibody. Following 1 h incubation, unbound biotin-conjugated anti-human TGFβ1 antibody was removed during a wash step. Then, streptavidin–horseradish peroxidase (HRP) was added. After 1 h incubation, unbound streptavidin–HRP was removed during a wash step and a substrate solution reactive with HRP was applied to the wells for around 15 min. A colored product was formed in proportion to the amount of human TGFβ1 present in the sample or standard. The reaction was terminated by addition of the stop solution. The absorbance was measured at 450 nm with a TECAN Spark with SparkControl megellan software v.2.2. (Tecan). A standard curve was prepared from seven human TGFβ1 standard dilutions and human TGFβ1 sample concentration were determined using Magellan software (Tecan).

Multiparametric flow cytometry

The following antibodies were used for multiparametric flow cytometry: anti-CD14-APC-eFluor780 (61D3, 1:100 dilution), anti-CD19-APC-eFluor780 (HIB19, 1:100 dilution), anti-EOMES-PE-Cy5.5 (WD1928, 1:800 dilution), anti-KLRG1-SuperBright702 (13F12F2, 1:50 dilution), anti-T-BET-PE-Cy7 (4B10, 1:200 dilution) and anti-TOX-eFluor660 (TRX10, 1:100 dilution) (all eBioscience). Anti-BLIMP1-PE-Dazzle (6D3, 1:25 dilution), anti-CD107a-APC (H4A3, 1:100 dilution), anti-CD38-BUV737 (HB7, 1:200 dilution), anti-CD45RA-BUV496 (HI100,1:200 dilution), anti-CD8-BUV395 (RPA-T8,1:200 dilution), anti-CD8-BUV496 (RPA-T8, 1:00 dilution), anti-CD8-BB515 (RPA-T8,1:100 dilution), anti-GZMB-BV510 (GB11, 1:100 dilution), anti-IFNγ-FITC (4 S.B3, 1:8 dilution), anti-Ki67-BV510 (B56, 1:20 dilution), anti-KLRD1-BV421 (HP-3D9, 1:200 dilution), anti-TNF-PE-Cy7 (MAb11, 1:50 dilution), anti-PD1-BV786 (EH12.1, 1:33 dilution) (all BD Bioscience). anti-CCR7-Ax700 (G043H7, 1:25 dilution), anti-CCR7-BV786 (G043H7, 1:33 dilution), anti-CD127-BV605 (A019D5, 1:33 dilution), anti-CD45RA-BV510 (HI100, 1:200 dilution), anti-rabbit IgG- FITC (Poly4064, 1:200 dilution), anti-rabbit IgG-PE-CF594 (Poly4064, 1:200 dilution) and anti-PRF1-BV711 (dG9, 1:200 dilution) (all BioLegend). Anti-ZEB2-AF647 (923328, 1:25 dilution, R&D), anti-NKG7-pure (polyclonal, 1:50 dilution, Biorybt) and anti-RUNX1/2/3-pure (SD0803, 1:800 dilution, Thermo Fisher). Fixable Viability Dyes APC-eFluor780 (1:200 dilution, eBioscience) was used for live/dead discrimination. Fixation/Permeabilization Solution kit (BD Biosciences) and FoxP3/Transcription Factor Staining Buffer Set (eBioscience) were applied according to the manufacturer's instructions to stain for cytoplasmic and intranuclear molecules, respectively. Cells were fixed with 2% paraformaldehyde (PFA; Sigma). Analyses were performed using FACS Canto II or LSRFortessa with FACSDiva software v.10.6.2 (BD). We performed a machine and measurement standardization procedure applying the CS&T system (BD Biosciences) to optimize and standardize cytometer setup and to receive reproducible data. Data were evaluated with FlowJo v.10 (Treestar). Only individuals harboring

≥80% non-naive HBV epitope-specific CD8$^+$ T cells and with at least ten cells were included in further analyses.

Dimensionality reduction of multiparameter flow cytometry data

The visualization of multiparametric flow cytometry data was conducted with R v.4.3.3. using the Bioconductor (release 3.18) CATALYST package (v.1.26.0)[53]. The analyses were performed on gated non-naive HBV epitope-specific CD8$^+$ T cells as well as non-naive GZMB$^+$ HBV pol$_{455}$-specific CD8$^+$ T cells. Analysis for Figs. 2e, 3d and 6h and Extended Data Figs. 2c and 8d included the markers GZMB, PRF1, NKG7, KLRD1, T-BET, EOMES, ZEB2, CD127, TOX and PD-1. Analysis for Fig. 5e and Extended Data Fig. 5a was performed on PRF1, NKG7, KLRD1, T-Bet, EOMES, ZEB2, CD127, TOX and PD-1. Downsampling of cells to 1,000 was performed before dimensionality reduction to facilitate the visualization of different samples. Marker intensities were transformed by arcsinh (inverse hyperbolic sine) with a cofactor of 150. Dimensionality reduction on the transformed data was achieved by t-SNE, MDS and diffusion map visualization.

Single-cell sorting for scRNA-seq by mCEL-seq2 approach

HBV epitope-specific CD8$^+$ T cells were enriched by magnetic bead-based enrichment, and surface staining was performed. Live HBV epitope-specific CD8$^+$ T cells were sorted in 384-well plates (Bio-Rad) containing lysis buffer and mineral oil using FACS Melody Cell Sorter with BD FACSChorus software v.3.4.1 (BD). Naive CD45RA$^+$CCR7$^+$ T cells were excluded. The sorter was run on single-cell sort mode. After the completion of sorting, the plates were centrifuged for 1 min at 2,200g at 4 °C, snap frozen in liquid nitrogen and stored at −80 °C until processing.

scRNA amplification and library preparation of mCEL-seq2 approach

scRNA-seq was performed using the mCEL-seq2 protocol, an automated and miniaturized version of CEL-seq2 on a mosquito nanoliter-scale liquid-handling robot (TTP LabTech)[24,54]. As reported previously, the CEL-seq2 protocol was established and optimized to analyze the heterogeneity of rare cells[54]. Libraries with 96 cells each were sequenced per lane on an Illumina HiSeq 3000 sequencing system (pair-end multiplexing run) at a depth of ~130,000–200,000 reads per cell.

Quantification of transcript abundance of mCEL-seq2 approach

Paired-end reads were aligned to the transcriptome using bwa (v.0.6.2-r126) with default parameters[55]. The transcriptome contained all gene models based on the human whole-genome ENCODE v.24 release. All isoforms of the same gene were merged to a single gene locus. Furthermore, gene loci overlapping by >75% were merged to larger gene groups. The right mate of each read pair was mapped to the ensemble of all gene loci and to the set of 92 External RNA Control Consortium spike-ins in the sense direction[56]. Reads mapping to multiple loci were discarded. The left read contains the barcode information: the first six bases corresponded to the unique molecular identifier (UMI) followed by six bases representing the cell-specific barcode. The remainder of the left read contains a polyT stretch. For each cell barcode, the number of UMIs per transcript was counted and aggregated across all transcripts derived from the same gene locus. Based on binomial statistics, the number of observed UMIs were converted into transcript counts[57].

scRNA-seq data analysis of mCEL-seq2 approach

Clustering analysis and visualization were performed using Seurat v.4.3.0[26]. Only protein coding genes were included in the downstream data analysis. Mitochondrial genes and genes encoding for small and large ribosomal subunits (Supplementary Fig. 1a) were excluded before

clustering. Cells with a total number of transcripts <1,000 (<500 for HBV core$_{18}$ data) were discarded, and count data of the remaining cells were normalized. As published previously for mCEL-seq2 approaches[24,25,58–60], cells expressing >1.5% of *KCNQ1OT1*, a potential marker for low-quality cells[61], were not considered for analysis. In brief, *KCNQ1OT1* serves as a non-cell-type-specific marker in several datasets analyzed across different tissues in mice and humans using mCEL-seq2 approach. Cells, also HBV-specific CD8$^+$ T cells, with a higher percentage of KCNQ1OT1 transcripts mainly represent low-quality cells with a significantly lower number of transcripts per cell (Supplementary Fig. 2). In particular, the genes correlating with KCNQ1OT1 were primarily long noncoding RNAs (AC006548.28, AC092669.3, ASTN2, ATP9B, BLOC1S6, C4orf32, HELLPAR, KIAA1328, LINC00504, LINC00506, LINC00976, MAB21L3, ORC4, RASEF, RP11-142G1.3, RP11-17A4.2, RP11-259O2.3, RP11-346D14.1, RP11-382B18.1, RP11-609N14.4, RP11-624A21.1, RP11-703G6.1, RP3-323A16.1, RP4-598P13.1, RPAP2, SOD2, SULT1B1, TBC1D8B, TMEM212, UGDH-AS1, WDPCP and Xbac-BPG154L12.4) and their inclusion or exclusion would not affect the results and findings of the study. Additionally, transcripts correlating to *KCNQ1OT1* with a Pearson's correlation coefficient > 0.65 were removed. We observed heterogeneity between participants in the dataset (Supplementary Fig. 3), which was corrected using the RunHarmony function of the Harmony package (v.0.1.1), which runs Harmony, a scRNA-seq data integration algorithm with a Seurat workflow[27]. Default parameters were used to run Seurat, except for cluster resolution (set to 0.5 for the integrative analysis of HCV and HBV data as well as the combined analysis HBV core$_{18}$ and HBV pol$_{455}$ data and 0.4 for the analysis of HBV pol$_{455}$ data). Cells from each participant were considered a batch. Dimensionality reduction for visualization was performed using the RunUMAP function where reduction parameter was set to 'harmony'. DEGs were calculated using the FindMarkers function of Seurat algorithm. Diffusion maps were created using the destiny R package (v.3.16.0)[31]. The top 2,000 variable genes obtained using the FindVariableFeatures function of Seurat were included in the diffusion map calculation. The number of nearest neighbors k was set to 10 and 50 principal components were used. Gene regulatory network inference on HBV pol$_{455}$ data was performed using SCENIC (v.1.3.1) with default settings. The weightThreshold was set to 0.006 in the runSCENIC_1_coexNetwork2modules function[32].

scRNA-seq by 10x Genomics approach

scRNA-seq was performed using 10x Genomics with feature barcoding technology to multiplex cells from different individuals so that they could be loaded on one well to reduce costs and minimize technical variability. Hashtag oligonucleotides were obtained as purified and already oligonucleotide-conjugated in TotalSeq-C (5′ chemistry) format from BioLegend. HBV pol$_{455}$-specific CD8$^+$ T cells were enriched by magnetic bead-based enrichment and surface staining was performed. Cells were stained with barcoded antibodies together with the surface staining solution. The antibody concentrations used were 1 μg per million cells, as recommended by the manufacturer (BioLegend). After staining, cells were washed three times in PBS (PAN Biotech) containing 2% BSA (AppliChem) and 0.01% Tween 20 (Merck KGaA) followed by centrifugation (300g for 5 min at 4 °C) and supernatant exchange. After the final wash, the cells were resuspended in PBS, filtered through 40-μm cell strainers and processed for sorting. Live HBV pol$_{455}$-specific CD8$^+$ T cells were sorted in 1.5-ml microcentrifuge tubes (Eppendorf) containing 20 μl PBS using BD Aria Fusion with FACSDiva software v.10.6.2 (BD). The 1.5-ml microcentrifuge tubes were coated with 5% BSA overnight and rinsed twice with 1 ml PBS before usage. Naive, CD45RA$^+$CCR7$^+$ T cells were excluded. The sorter was run on purity sort mode. Sorted cells were processed through the 10x Genomics single-cell workflow according to the manufacturer's instructions. Libraries were pooled to desired quantities to obtain appropriate sequencing depths as recommended by 10x Genomics and sequenced on a NovaSeq 6000 flow cell.

Quantification of transcript abundance of 10x Genomics approach

Quantification of gene expression and cell surface protein abundance counts was performed using Cell Ranger v.6.0.0 using the count command, which performs alignment, filtering, barcode counting and UMI counting as well as processing feature barcoding data. Alignment was performed using a prebuilt Cell Ranger human reference GRCh38 (GENCODE v.32/Ensembl 98).

scRNA-seq data analysis of 10x Genomics approach

Clustering analysis and visualization were performed using Seurat v.4.3.0 (ref. 26). Demultiplexing of the hashtag oligonucleotides was performed using HTODemux function with positive.quantile set to 0.99. Mitochondrial genes and genes encoding for small and large ribosomal subunits (Supplementary Fig. 1b) as well as T cell receptor α, β, γ and δ (TRA, TRB, TRG and TRD) were excluded before clustering. Cells with a total number of transcripts <500 and expressing >10% of mitochondrial genes were discarded and count data of the remaining cells were normalized. We observed heterogeneity between participants in the dataset, which was corrected using the RunHarmony function of the harmony package (v.0.1.1) which runs Harmony, a scRNA-seq data integration algorithm with the Seurat workflow[27]. Default parameters were used to run Seurat, except that cluster resolution was set to 0.6. Cells from each participant were considered as a batch. Dimensionality reduction for visualization was performed using RunUMAP function where reduction parameter was set to 'harmony'. DEGs were calculated using the FindAllMarkers function of Seurat algorithm. Gene regulatory network inference was performed using SCENIC (v.1.3.1) with default settings. The weightThreshold was set to 0.004 in the runSCENIC_1_coexNetwork2modules function[32].

Statistics

Statistical analysis was performed with GraphPad Prism v.10 (GraphPad Prism Software) and R v.4.3.3. Statistical significance was assessed by a Kruskal–Wallis test, including Dunn's multiple comparisons test, two-tailed Mann–Whitney comparison tests, simple linear regression analysis and two-tailed Wilcoxon matched-pairs signed-rank test. Analyses were performed in independent experiments.

Reporting summary

Further information on research design is available in the Nature Portfolio Reporting Summary linked to this article.

Data availability

The expression count files for the scRNA-seq data of HBV epitope-specific CD8$^+$ T cells reported in this paper are available to download from the Gene Expression Omnibus under accession number GSE259231. Processed data can be downloaded from https://github.com/sagar161286/HBV2024. The scRNA-seq data of HCV-specific CD8$^+$ T cells used for comparison were downloaded under accession number GSE150305 (https://doi.org/10.1038/s41590-020-00817-w). For the alignment of scRNA-seq data, Cell Ranger human reference GRCh38 (GENCODE v.32/Ensembl 98) was used for the 10x Genomics approach. The gene sets for GSEA were downloaded from ref. 17 (exhaustion (chronic TCF-1$^-$), memory-like (chronic TCF-1$^+$) and memory signature), ref. 25 (cytotoxicity signature) or GO:0002369 (https://www.gsea-msigdb.org/gsea/msigdb/mouse/geneset/GOBP_T_CELL_CYTOKINE_PRODUCTION.html and *IFNG*, *TNF* and *IL2* were added), for IL-10 pathway genes (https://www.gsea-msigdb.org/gsea/msigdb/cards/BIOCARTA_IL10_PATHWAY), for IL-2 pathway genes (https://www.gsea-msigdb.org/gsea/msigdb/cards/BIOCARTA_IL2_PATHWAY), for IL-12 pathway genes (https://www.gsea-msigdb.org/gsea/msigdb/human/geneset/BIOCARTA_IL12_PATHWAY.html) and for type I IFN pathway genes (https://www.gsea-msigdb.org/gsea/msigdb/cards/ST_TYPE_I_INTERFERON_PATHWAY). The scRNA-seq data of liver FNAs

and blood used for comparison were downloaded under accession number GSE234241 (ref. 34). HBV wild-type reference sequences used for analyzing the HBV viral sequencing data were downloaded with NCBI accession codes: genotype A X02763, genotype D X02496 and genotype E X75657. Raw data in this study are provided in Source data. Source data are provided with this paper.

Code availability

Codes to reproduce the scRNA-seq data analysis and the analyses of multiparametric flow cytometry data and figures are available at https://github.com/sagar161286/HBV2024.

References

53. Crowell H. L., Zanotelli, V. R. T., Chevrier S., Robinson M. CATALYST: Cytometry dATa anALYSis Tools. R package version 1.15.0 https://github.com/HelenaLC/CATALYST (2020).
54. Hashimshony, T. et al. CEL-Seq2: sensitive highly-multiplexed single-cell RNA-seq. *Genome Biol.* **17**, 77 (2016).
55. Li, H. & Durbin, R. Fast and accurate long-read alignment with Burrows-Wheeler transform. *Bioinformatics* **26**, 589–595 (2010).
56. Baker, S. C. et al. The External RNA Controls Consortium: a progress report. *Nat. Methods* **2**, 731–734 (2005).
57. Grun, D., Kester, L. & van Oudenaarden, A. Validation of noise models for single-cell transcriptomics. *Nat. Methods* **11**, 637–640 (2014).
58. Aizarani, N. et al. A human liver cell atlas reveals heterogeneity and epithelial progenitors. *Nature* **572**, 199–204 (2019).
59. Sankowski, R. et al. Mapping microglia states in the human brain through the integration of high-dimensional techniques. *Nat. Neurosci.* **22**, 2098–2110 (2019).
60. Nusser, A. et al. Developmental dynamics of two bipotent thymic epithelial progenitor types. *Nature* **606**, 165–171 (2022).
61. Grun, D. et al. De novo prediction of stem cell identity using single-cell transcriptome data. *Cell Stem Cell* **19**, 266–277 (2016).

Acknowledgements

Author contributions

K.H. planned, performed and analyzed the experiments except for the computational analysis of scRNA-seq data. S. performed the scRNA-seq experiments together with K.H. and analyzed the scRNA-seq data. S.K. and Ö.S. contributed to the experiments. S.L.-L., D.A.P., A.R.M.K. and M.C. provided resources. F.E. performed four-digit HLA-typing by next-generation sequencing. D.W., P.K., T.B., B.B. and C.N.H. contributed to data interpretation. M.H. and R.T. designed and supervised the study, contributed to experimental design and planning, interpreted data and wrote the manuscript, together with K.H.

Competing interests

The authors declare no competing interests.

Additional information

Extended data is available for this paper at https://doi.org/10.1038/s41590-024-01928-4.

Supplementary information The online version contains supplementary material available at https://doi.org/10.1038/s41590-024-01928-4.

Correspondence and requests for materials should be addressed to Robert Thimme or Maike Hofmann.

Peer review information *Nature Immunology* thanks Matteo Iannacone, Mala Maini, and the other, anonymous, reviewer(s) for their contribution to the peer review of this work. Primary Handling Editor: P. Jauregui, in collaboration with the *Nature Immunology* team. Peer reviewer reports are available.

Reprints and permissions information is available at www.nature.com/reprints.

a

b

c

d
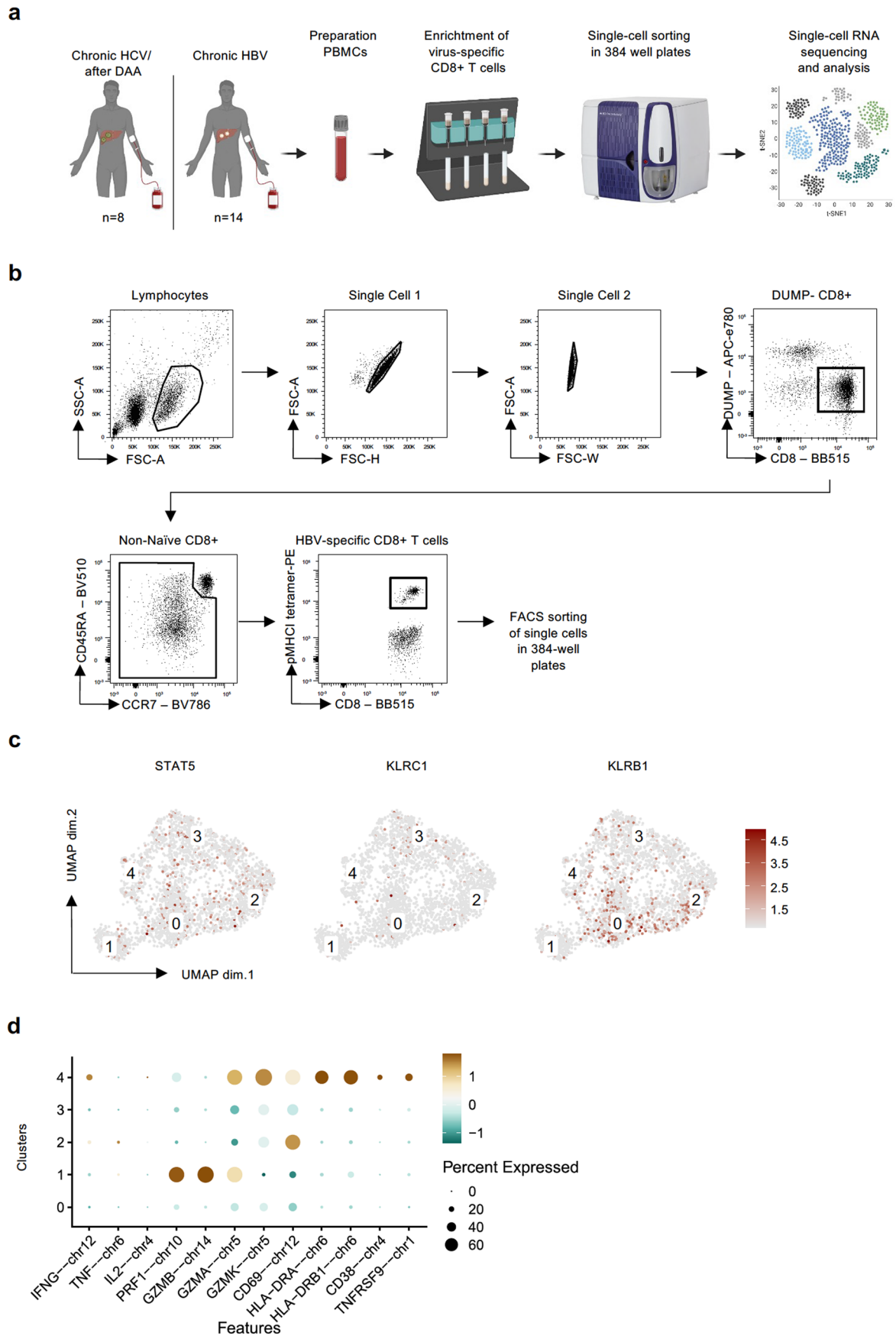
Extended Data Fig. 1 | See next page for caption.

Extended Data Fig. 1 | Experimental setup of scRNAseq analysis using mCEL-seq2. (a) Study design is illustrated. Comprehensive analysis of the single-cell transcriptomes of HCV-specific CD8 $^+$ T cells from individuals infected with chronic HCV (n = 6) and after DAA-mediated cure of chronic HCV infection (n = 2) versus HBV-specific CD8 T cells from chronic HBV-infected individuals (n = 14) were performed by using the mCEL-seq2 technology. **(b)** Gating strategy of flow cytometry-based cell sorting of HBV-specific CD8 $^+$ T cells for scRNA-seq: after lymphocyte gating and two-way doublet exclusion, live CD8 $^+$ T cells were gated.

Naïve CD8 $^+$ T cells (CD45RA + CCR7 +) were excluded and HLA-A*02:01-restricted HBV-specific CD8 $^+$ T cells were identified by peptide-loaded HLA class I tetramer and then sorted into 384-well plates. **(c)** Feature plots showing gene expression of STAT5, KLRC1 and KLRB1 genes in C0–4. Scaled expression is depicted (gray, low; red, high). **(d)** Heatmap showing the expression of cytokines, cytotoxic markers and activation-related genes within the virus-specific CD8 + T cell clusters. Scaled expression levels are color coded (blue, low; brown, high).
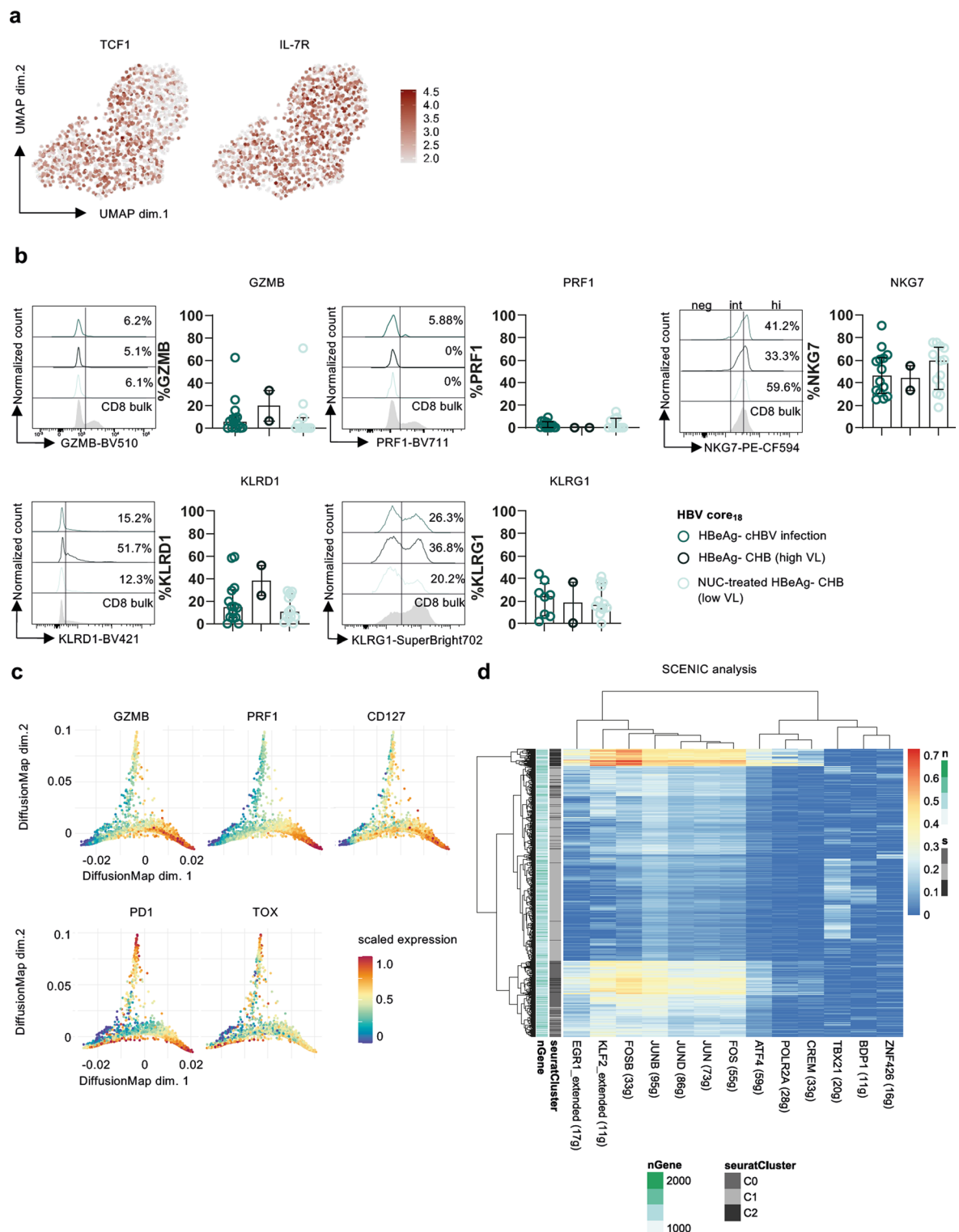
Extended Data Fig. 2 | Phenotypic and transcriptional characteristics of HBV-specific CD8⁺ T cells. (a) Feature plots showing *TCF7* and *IL7R* gene expression in C0–2 of HBV pol_{455}-specific CD8⁺ T cells (endogenous control/chronic HBV n = 3, NUC control/chronic HBV n = 4). Scaled expression is depicted (gray, low; red, high). (b) Expression analysis of cytotoxic molecules (GZMB and PRF1), the cytolytic regulator NKG7 as well as the C-type lectin-like NK cell receptors KLRD1 and KLRG1 was performed in peptide-loaded/HLA class I tetramer-enriched HBV $core_{18}$-specific CD8⁺ T cells from chronic HBV-infected individuals (for GZMB, PRF1, NKG7, KLRD1: endogenous control/ chronic HBV, low viral load, dark green, n = 14; high viral load, dark green/black, n = 2; NUC control/chronic HBV, low viral load, light green, n = 11; for KLRG1: endogenous control/ chronic HBV, low viral load, dark green, n = 8; high viral load, dark green/black, n = 2;

NUC control/chronic HBV, low viral load, light green, n = 12). Representative histograms including gating of the individual markers are displayed. Each dot represents one HBV $core_{18}$-specific CD8⁺ T cell response and with color coding as indicated. Bar charts show the median value with IQR. (c) Expression levels of indicated markers are plotted on the diffusion map (blue, low; red, high) (endogenous control/ chronic HBV, low viral load, dark green, n = 12; high viral load, dark green/black, n = 4; NUC control/chronic HBV, low viral load, light green, n = 14). (d) Regulon activity matrix obtained from single-cell transcriptomes of HBV pol_{455}-specific CD8⁺ T cells of chronically HBV-infected individuals (endogenous control/chronic HBV n = 3, NUC control/chronic HBV n = 4) after applying SCENIC algorithm. Statistical significance was assessed by a Kruskal–Wallis test including Dunn's multiple comparisons test (b).
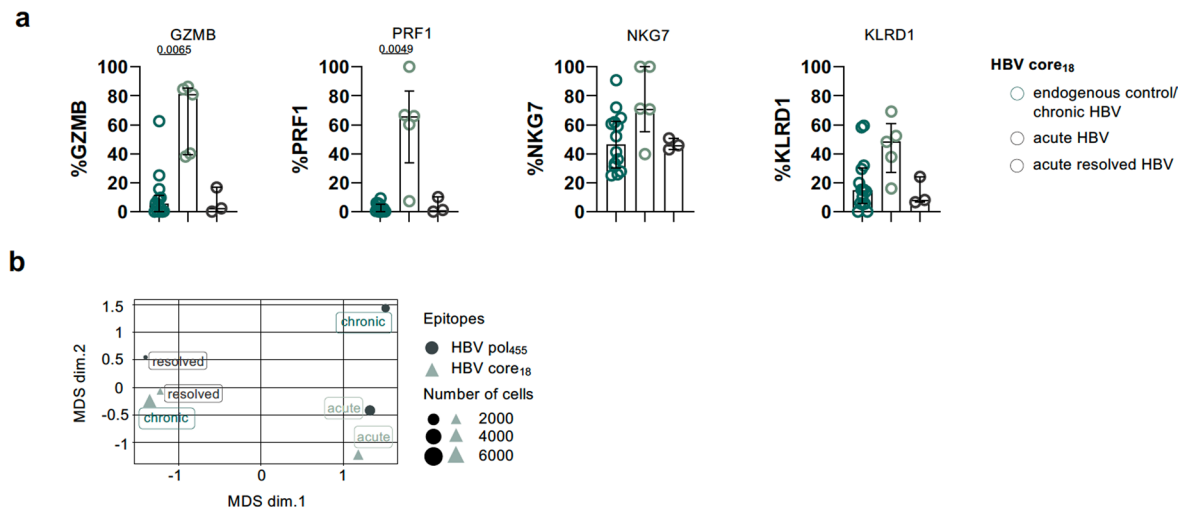
Extended Data Fig. 3 | Cytotoxic characteristics of HBV core18-versus HBV pol455-specific CD8+ T cells. (a) Flow cytometric analysis of the cytotoxic molecules GZMB and PRF1, the cytolytic regulator NKG7 as well as the C-type lectin-like NK cell receptor KLRD1 in HBV core$_{18}$-specific CD8+ T cells from these cohorts is shown. Statistical graph depicts frequencies of HBV core$_{18}$-specific CD8+ T cells. Each dot represents one of the respective HBV core$_{18}$-specific CD8+ T cell responses with color coding as indicated: dark green, endogenous control/ chronic HBV, n = 14; light green, acute HBV, n = 5; dark gray, acute resolved HBV, n = 3. **(b)** MDS representation of concatenated flow cytometry data gated on HBV core$_{18}$-specific and HBV pol$_{455}$-specific CD8+ T cells of acute (n = 12; HBV core$_{18}$: n = 5, HBV pol$_{455}$: n = 7), acute resolved (n = 7; HBV core$_{18}$: n = 3, HBV pol$_{455}$: n = 4) and endogenous control/chronic HBV infection (n = 26; HBV core$_{18}$: n = 14, HBV pol$_{455}$: n = 12) is illustrated. Bar charts show the median value with IQR. Statistical significance was assessed by a Kruskal–Wallis test including Dunn's multiple comparisons test (a).
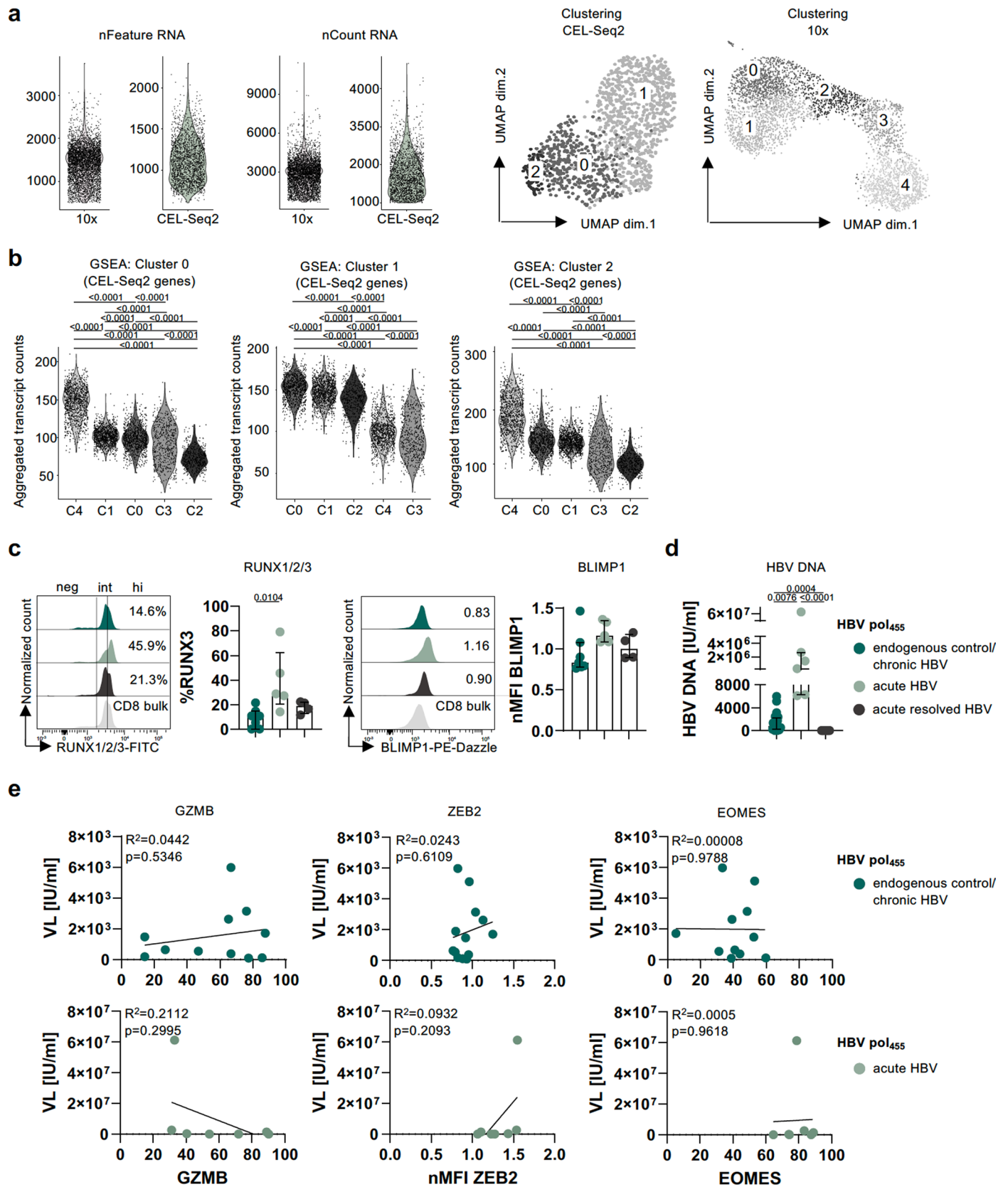
Extended Data Fig. 4 | See next page for caption.

Extended Data Fig. 4 | Distinct cytotoxic HBV pol455-specific CD8⁺ T cell responses in endogenously controlled versus acute HBV infection.
(a) Comparison of mCEL-seq2 (endogenous control/chronic HBV, n = 3; NUC control/chronic HBV, n = 4) and 10x Genomics scRNA-seq data (endogenous control/chronic HBV, n = 3; acute HBV, n = 3; acute resolved HBV, n = 2) are illustrated. nFeature RNA, nCount RNA and the clustering are depicted.
(b) Comparison of C0–4 identified with 10x scRNA-seq with cluster signatures defined in the mCEL-seq2 approach by GSEA. (c) The transcription factors RUNX3 and BLIMP1 were assessed in HBV pol$_{455}$-specific CD8⁺ T cells of different cohorts (endogenous control/chronic HBV, n = 7; acute HBV, n = 5; acute resolved HBV, n = 4). Histograms and statistical graph depicting gating and frequencies of HBV

pol$_{455}$-specific CD8⁺ T cells are displayed. (d) Serum HBV DNA in endogenous control/chronic HBV (n = 24) versus acute HBV (n = 8) and acute resolved HBV (n = 11) are depicted. (e) Correlation analyses of viral load and the frequency of HBV pol$_{455}$-specific CD8⁺ T cells expressing GZMB, ZEB2, EOMES obtained from individuals within endogenous control/chronic HBV (for GZMB and EOMES: n = 11; for ZEB2: n = 13) or acute HBV (n = 7) are depicted, respectively. Each dot represents one HBV pol$_{455}$-specific CD8⁺ T cell response with color coding as indicated: dark green, in endogenous control/chronic HBV; light green, acute HBV; dark gray, acute resolved HBV. Bar charts show the median value with IQR. Statistical analyses were performed via Kruskal–Wallis test including Dunn's multiple comparisons test (b,c,d) and simple linear regression analysis (e).
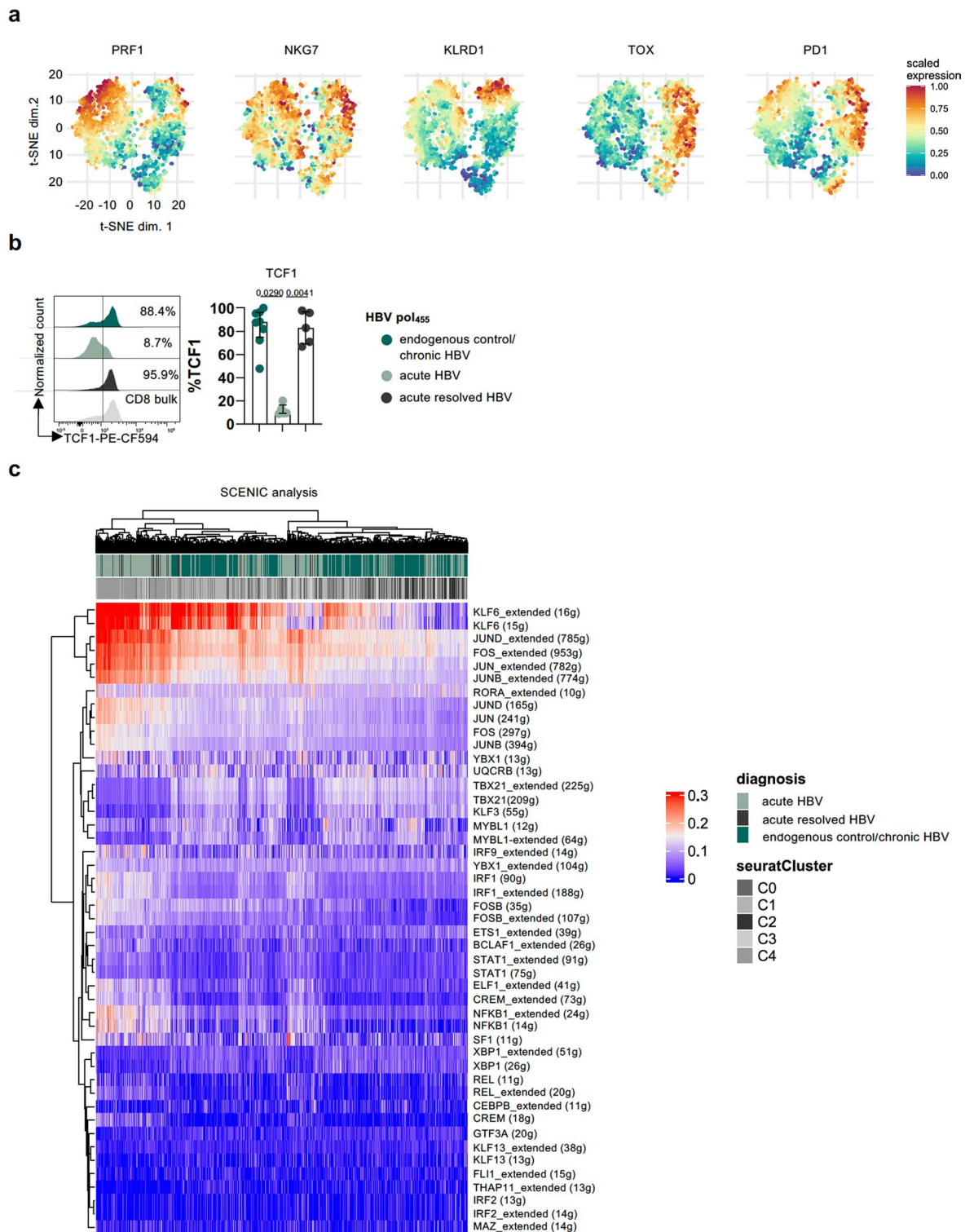
Extended Data Fig. 5 | Characteristics of HBV pol455-specific CD8⁺ T cells in endogenously controlled vs. acute. vs acute resolved HBV infection.
(a) Protein expression levels of the indicated cytotoxic- and exhaustion-associated markers in GZMB⁺ HBV pol$_{455}$-specific CD8⁺ T cells are plotted on t-SNE (endogenous control/chronic HBV, n = 12; acute HBV, n = 7; acute resolved HBV, n = 4). Scaled expression (blue, low; red, high) is depicted.
(b) Expression levels of TCF-1 were examined in HBV pol$_{455}$-specific CD8⁺ T cells t-SNE (endogenous control/chronic HBV, n = 8; acute HBV, n = 4; acute resolved HBV, n = 5). Histograms and statistical graph depicting gating and frequencies of HBV pol$_{455}$-specific CD8⁺ T cells are displayed. (c) Regulon activity matrix obtained from single-cell transcriptomes of HBV pol$_{455}$-specific CD8⁺ T cells in endogenous control/chronic HBV (n = 3), acute HBV (n = 3) and acute resolved HBV infection (n = 2) after applying SCENIC algorithm. Each dot represents one HBV pol$_{455}$-specific CD8⁺ T cell response with color coding as indicated: dark green, in endogenous control/chronic HBV; light green, acute HBV; dark gray, acute resolved HBV. Bar charts show the median value with IQR. Statistical analyses were performed via Kruskal–Wallis test including Dunn's multiple comparisons test (b).
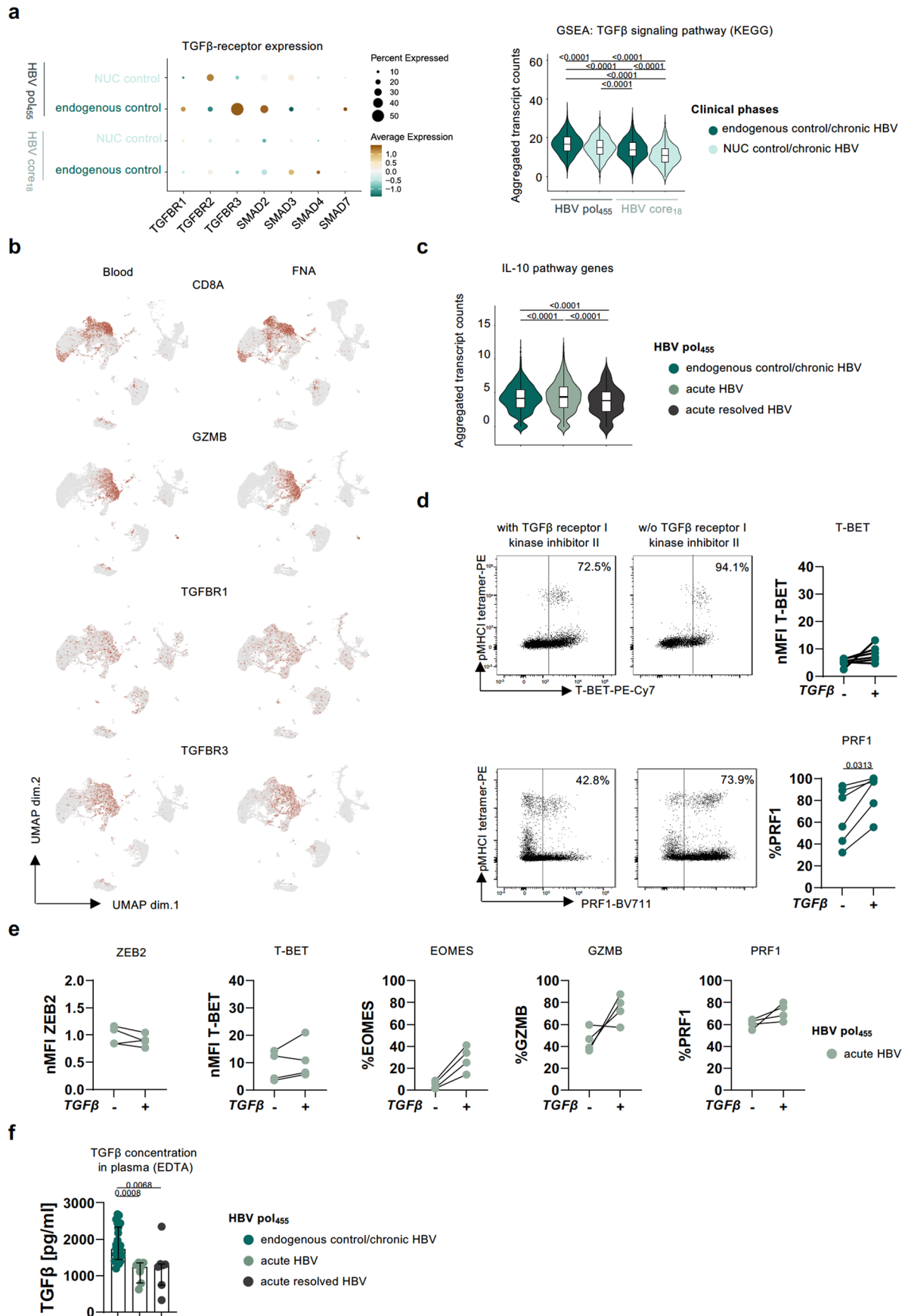
Extended Data Fig. 6 | See next page for caption.

**Extended Data Fig. 6 | TGFß pathway analyses of HBV-specific CD8$^+$ T cells.**
(a) Heatmap showing TGFβ-receptor gene expression in HBV core$_{18}$-specific and HBV pol$_{455}$-specific CD8$^+$ T cells of endogenous control/chronic HBV (n = 7; HBVcore$_{18}$: n = 4, HBVpol$_{455}$: n = 3) and NUC control/chronic HBV (n = 7; HBVcore$_{18}$: n = 3, HBVpol$_{455}$: n = 4) (left). Scaled expression levels are color coded (blue, low; brown, high). GSEA analysis of the TGFβ signaling pathway in HBV core$_{18}$-specific versus HBV pol$_{455}$-specific CD8$^+$ T cells of endogenous control/chronic HBV and NUC control/chronic HBV (right). The aggregated transcript counts are mapped in violin plots (box center line, median; box limits, upper and lower quartiles; box whiskers, IQR). **(b)** Feature plots showing CD8A, GZMB, TGFBR1 and TGFBR3 co-expression in CD8$^+$ T cells sampled from blood and the liver by FNA (data from Genshaft et al., Hepatology, 2023). **(c)** IL-10 cytokine pathway gene expression analysis of HBV pol$_{455}$-specific CD8$^+$ T cells obtained from endogenous control/chronic HBV (n = 3), acute HBV (n = 3) and acute resolved HBV infection (n = 2).

The aggregated transcript counts are mapped in violin plots (box center line, median; box limits, upper and lower quartiles; box whiskers, IQR). **(d)** Dot plots showing T-BET and PRF1 expression of HBV pol$_{455}$-specific CD8$^+$ T cells obtained from endogenous control/chronic HBV (n = 6) after 14 days of in vitro culture with (left) and without TGF-β RI Kinase Inhibitor II (right). Statistical graph depicting frequencies of T-BET+ or PRF1 + HBV pol$_{455}$-specific CD8$^+$ T cells are displayed. **(e)** ZEB2, T-BET, EOMES, GZMB and PRF1 expression of HBV pol$_{455}$-specific CD8$^+$ T cells obtained from acute HBV infection (n = 4) after 14 days of in vitro culture with and without TGF-β RI Kinase Inhibitor II is shown. **(f)** TGFβ concentration in plasma (EDTA) in endogenous control/chronic HBV (n = 26), acute HBV (n = 7) and acute resolved HBV (n = 7) was determined by ELISA and is depicted as pg/ml. Bar charts show the median value with IQR. Statistical analyses were performed via Kruskal–Wallis test including Dunn's multiple comparisons test (a,c,f) and two-tailed Wilcoxon matched-pairs signed rank test (d,e).
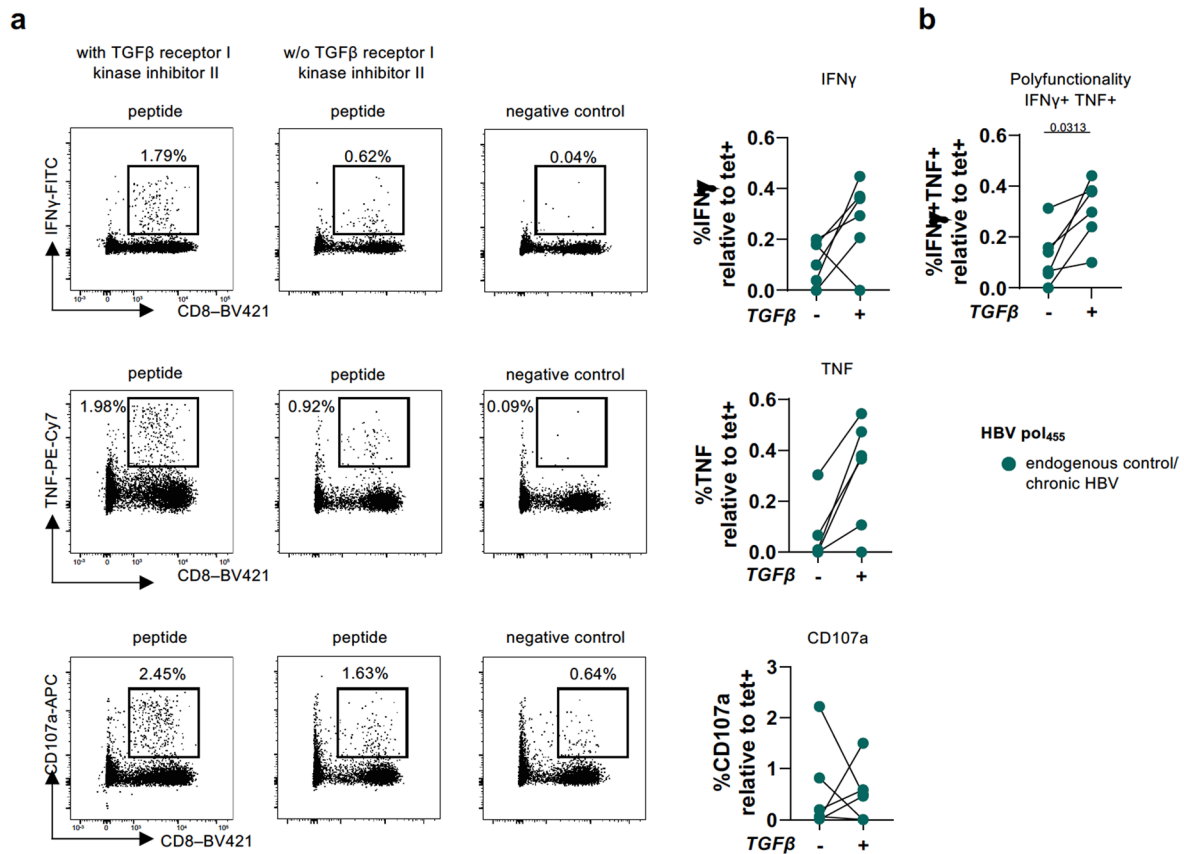
Extended Data Fig. 7 | Impact of TGFβ signalling inhibition on HBV pol455-specific CD8⁺ T cell function. (a) Dot plots showing IFNγ-, TNF and CD107a-producing HBV pol$_{455}$-specific CD8⁺ T cells in response to peptide stimulation after 14 days of in vitro culture with (left) and without TGFβ RI Kinase Inhibitor II (middle). Negative control is depicted on the right. The percentages of IFN-γ-, TNF and CD107a-producing HBV pol$_{455}$-specific CD8⁺ T cells were determined in relation to the frequency of HBV pol$_{455}$-specific CD8⁺ T cells for individuals with endogenous control/chronic HBV. **(b)** The polyfunctionality of HBV pol$_{455}$-specific CD8⁺ T cells were assessed by gating on IFN-γ and TNF positive cells. Each dot represents one of the respective HBV pol$_{455}$-specific CD8 ⁺ T cell responses with color coding as indicated: dark green, endogenous control/chronic HBV, n = 6. Statistical analyses were performed via two-tailed Wilcoxon matched-pairs signed rank test (a,b).
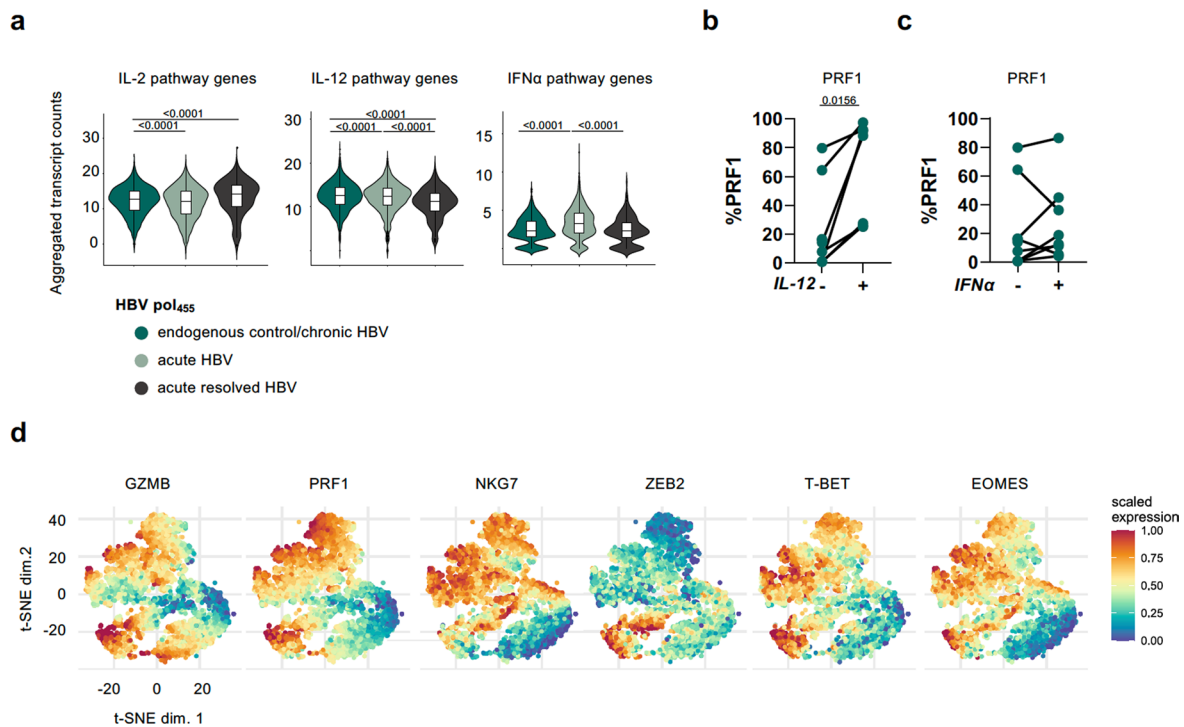
Extended Data Fig. 8 | Effects of IL12 and IFNα on the attenuated HBV pol$_{455}$-specific CD8$^+$ T cell response. (a) IL-2, IL-12 and IFNα cytokine pathway gene expression analysis of HBV pol$_{455}$-specific CD8$^+$ T cells obtained from endogenous control/chronic HBV (n = 3), acute HBV (n = 3) and acute resolved HBV infection (n = 2). The aggregated transcript counts are mapped in violin plots (box center line, median; box limits, upper and lower quartiles; box whiskers, IQR). **(b+c)** PRF1 expression of HBV pol$_{455}$-specific CD8$^+$ T cells after 14 days of in vitro culture with **(b)** IL-12 (endogenous control/chronic HBV n = 7) or **(c)** IFNα treatment (endogenous control/chronic HBV n = 8) or without any treatment is shown **(d)** Protein expression levels of the indicated cytotoxic and effector-associated markers in HBV pol$_{455}$-specific CD8$^+$ T cells are plotted. Scaled expression (blue, low; red, high) is depicted. Each dot represents one of the respective HBV pol$_{455}$-specific CD8$^+$ T cell responses with color coding as indicated: dark green, endogenous control/chronic HBV. Statistical analyses were performed via Kruskal–Wallis test including Dunn's multiple comparisons test (a) and two-tailed Wilcoxon matched-pairs signed rank test (b,c).

nature portfolio

Corresponding author(s):	Robert Thimme, MD Maike Hofmann, PhD
Last updated by author(s):	02.07.2024

Reporting Summary

Nature Portfolio wishes to improve the reproducibility of the work that we publish. This form provides structure for consistency and transparency in reporting. For further information on Nature Portfolio policies, see our Editorial Policies and the Editorial Policy Checklist.

Statistics

For all statistical analyses, confirm that the following items are present in the figure legend, table legend, main text, or Methods section.

n/a	Confirmed	
☐	☒	The exact sample size (*n*) for each experimental group/condition, given as a discrete number and unit of measurement
☐	☒	A statement on whether measurements were taken from distinct samples or whether the same sample was measured repeatedly
☐	☒	The statistical test(s) used AND whether they are one- or two-sided *Only common tests should be described solely by name; describe more complex techniques in the Methods section.*
☒	☐	A description of all covariates tested
☐	☒	A description of any assumptions or corrections, such as tests of normality and adjustment for multiple comparisons
☐	☒	A full description of the statistical parameters including central tendency (e.g. means) or other basic estimates (e.g. regression coefficient) AND variation (e.g. standard deviation) or associated estimates of uncertainty (e.g. confidence intervals)
☐	☒	For null hypothesis testing, the test statistic (e.g. *F*, *t*, *r*) with confidence intervals, effect sizes, degrees of freedom and *P* value noted *Give P values as exact values whenever suitable.*
☐	☒	For Bayesian analysis, information on the choice of priors and Markov chain Monte Carlo settings
☐	☒	For hierarchical and complex designs, identification of the appropriate level for tests and full reporting of outcomes
☐	☒	Estimates of effect sizes (e.g. Cohen's *d*, Pearson's *r*), indicating how they were calculated

Our web collection on statistics for biologists contains articles on many of the points above.

Software and code

Policy information about availability of computer code

Data collection	All software used to perform data collection are described in the methods section of the manuscript. Multiparametric flow cytometry data was collected on FACS Canto II and LSRFortessa with FACSDiva software version 10.6.2 (BD, Germany). FACS sorting was done on FACS Melody Cell Sorter with BD FACSChorus software version 3.4.1 (BD, Germany) and BD Aria Fusion with FACSDiva software version 10.6.2 (BD, Germany). ELISA data was collected by SparkControl magellan software version 2.2.
Data analysis	All codes used to perform bioinformatic analyses are described in the methods section of the manuscript or the supportive information. Multiparametric flow cytometry data was analyzed using FlowJo software version 10.6.2 (Treestar, Becton Dickinson). The visualization of multiparametric flow cytometry data was done with R version 4.3.3 using the Bioconductor packages (version: Release (3.18)) and Catalyst packages (Crowell H, Zanotelli V, Chevrier S, Robinson M (2023). CATALYST: Cytometry dATa anALYSis Tools. doi:10.18129/B9.bioc.CATALYST; https://bioconductor.org/packages/CATALYST; version 1.26.0). ScRNA-seq data analysis was done with R versions 4.1.3, 4.2.2, 4.3.3 using the bwa (version 0.6.2-r126), Seurat (version 4.3.0), Harmony (version 0.1.1), destiny (version 3.16.0) and SCENIC (version 1.3.1) packages. Codes to reproduce the scRNA-seq data analysis and the analyses of multiparametric flow cytometry data and figures are available at: https://github.com/sagar161286/HBV2024. Visualization and statistical analysis was performed using GraphPad 10 software.

For manuscripts utilizing custom algorithms or software that are central to the research but not yet described in published literature, software must be made available to editors and reviewers. We strongly encourage code deposition in a community repository (e.g. GitHub). See the Nature Portfolio guidelines for submitting code & software for further information.

Data

All manuscripts must include a data availability statement. This statement should provide the following information, where applicable:

- Accession codes, unique identifiers, or web links for publicly available datasets
- A description of any restrictions on data availability
- For clinical datasets or third party data, please ensure that the statement adheres to our policy

The expression count files for the scRNA-seq data of HBV epitope-specific CD8+ T cells reported in this paper are available to download from the Gene Expression Omnibus (GEO) under accession number GSE259231 . Processed data can be downloaded from https://github.com/sagar161286/HBV2024. The scRNA-seq data of HCV-specific CD8+ T cells used for comparison were downloaded under accession number GSE150305 (https://doi.org/10.1038/s41590-020-00817). For the alignment of scRNA-sequencing data Cell Ranger human reference GRCh38 (GENCODE v32/Ensembl 98) was used for 10x genomics approach.The gene sets for GSEA were downloaded from https://doi.org/10.1016/j.immuni.2016.07.021 (exhaustion (chronic TCF-1−), memory-like (chronic TCF-1+) and memory signature), https://www.nature.com/articles/s41590-020-00817-w (cytotoxicity signature) or GO:0002369 (https://www.gsea-msigdb.org/gsea/msigdb/mouse/geneset/ GOBP_T_CELL_CYTOKINE_PRODUCTION.html and IFNG, TNF and IL2 were added), for IL-10 pathway genes (https://www.gsea-msigdb.org/gsea/ msigdb/cards/ BIOCARTA_IL10_PATHWAY), for IL-2 pathway genes (https://www.gsea-msigdb.org/gsea/msigdb/cards/BIOCARTA_IL2_PATHWAY), for IL-12 pathway genes (https://www.gsea-msigdb.org/gsea/msigdb/human/geneset/BIOCARTA_IL12_PATHWAY.ht ml) and for type I IFN pathway genes (https://www.gsea-msigdb.org/ gsea/msigdb /cards/ST_TYPE_I_INTERFERON_PATHWAY). The scRNA-seq data of liver fine-needle aspirates and blood used for comparison were downloaded under accession number GSE234241 (https://doi.org/10.1097/HEP.0000000000000438). HBV wildtype reference sequences used for analyzing the HBV viral sequencing data were downloaded with the NCBI accession codes: genotype A X02763, genotype D X02496, genotype E X75657.
Raw data in this study are provided in the Source data.

Research involving human participants, their data, or biological material

Reporting on sex and gender	The sexes male and female have been included into this study and reported in Extended Data Table 4 as clinically documented. No sex-based analyses have been performed in this study due to sample restrictions.
Reporting on race, ethnicity, or other socially relevant groupings	The variables race, ethnicity or other socially relevant groupings have not been integrated in this study.
Population characteristics	HLA-A*02:01-positive individuals with endogenous controlled chronic HBV infection: Median age: 38 years, sex ratio m/f: 29/14, Median Viral Load: 640 IU/ml; Median ALT/AST values: 24/22.5 IU/ml. HLA-A*35:01-positive individuals with endogenous controlled chronic HBV infection: Median age: 49 years, sex ratio m/f: 2/5, Median Viral Load: 309 IU/ml; Median ALT/AST values: 20/22 IU/ml. Median age of HLA-A*02:01-positive individuals with chronic HBV/high VL: Median age: 41.5 years, sex ratio m/f: 5/5, Median Viral Load: 51895 IU/ml; Median ALT/AST values: 30/36.5 IU/ml. HLA-A*02:01-positive individuals with NUC control/chronic HBV: Median age: 55 years, sex ratio m/f: 18/9, Median Viral Load: negative; Median ALT/AST values: 27/30 IU/ml. HLA-A*02:01-positive individuals with acute HBV infection: Median age: 41 years, sex ratio m/f: 7/1, Median Viral Load: 152206.5 IU/ml; Median ALT/AST values: 1697/3614 IU/ml. HLA-A*02:01-positive individuals with acute resolved HBV infection: Median age: 52 years, sex ratio m/f: 8/3, Median Viral Load: negative; Median ALT/AST values: 25/22 IU/ml.
Recruitment	Blood samples of participants with chronic, acute and acute resolved HBV infection were recruited at the Department of Medicine II of the University Hospital Freiburg, Germany and at the Department of Gastroenterology, Hepatology, Infectious Diseases and Endocrinology and at Hannover Medical School, Hannover, Germany.Samples were banked and selected according to the following criteria: HLA-A*02:01, HLA*B35:01, no liver cirrhosis, detectability of HBV-specific CD8+ T cells.
Ethics oversight	Written informed consent was obtained from all participants prior blood donation. The study was conducted according to federal guidelines, local ethics committee regulations of Albert-Ludwigs-Universität, Freiburg, Germany (no. 474/14, 384/18) and Hannover Medical School, Hannover, Germany (no. 3374-2016) and the Declaration of Helsinki (1975).

Note that full information on the approval of the study protocol must also be provided in the manuscript.

Field-specific reporting

Please select the one below that is the best fit for your research. If you are not sure, read the appropriate sections before making your selection.

☒ Life sciences ☐ Behavioural & social sciences ☐ Ecological, evolutionary & environmental sciences

For a reference copy of the document with all sections, see nature.com/documents/nr-reporting-summary-flat.pdf

Life sciences study design

All studies must disclose on these points even when the disclosure is negative.

Sample size

Patients were recruited and patient material was banked at the Department of Medicine II of the University Hospital Freiburg, Germany and at the Department of Gastroenterology, Hepatology, Infectious Diseases and Endocrinology and at Hannover Medical School, Hannover, Germany; inclusion criteria were: (1) 80 HLA-A*02:01-positive individuals with chronic HBV infection in different phases of infection: HBeAg-cHBV infection phase (referred as endogenous control/chronic HBV; n=43), HBeAg- CHB phase with high viral load (referred as chronic HBV/high VL, n=10) or HBeAg- CHB phase under NUC treatment (referred as NUC control/chronic HBV, n=27). (2) 14 HLA-B*35:01-positive individuals with chronic HBV infection in different phases of infection: HBeAg- cHBV infection phase (referred as endogenous control/chronic HBV; n=7) and HBeAg- CHB phase under NUC treatment (referred as NUC control/chronic HBV, n=7). (3) 8 HLA-A*02:01-positive individuals with acute HBV infection. (4) 11 HLA-A*02:01-positive individuals who resolved an acute HBV infection. Individuals were classified into different clinical phases of HBV infection according to EASL guideline o which considers the presence of HBeAg, HBsAg, HBV DNA levels, transaminase levels (ALT and AST), and the presence or absence of liver inflammation. Written informed consent was obtained from all participants prior blood donation.

The sample sizes are comparable to many other studies in the research field of human immunology and proved to be sufficient for the generation of reproducible results.

Data exclusions

For flow cytometrical analysis, inidividuals harbouring ≤80% non-naive HBV epitope-specific CD8+ T cells cell and with less than 10 cells were excluded. This data exclusion strategy has been applied and validated previously by our group to gain reproducible results in studies investigating virus-specific CD8+ T cells in human viral infections. Moreover, T cell responses of patients harboring viral sequence mutations in the targeted epitope were excluded.

Replication

Analyses were performed in independent experiments. Findings were reproducible.
scRNAseq analysis using mCEL-seq2:
7 individuals with endogenous control/chronic HBV for HLA*02:01/HBVpol455 (n=3) and HLA*02:01/HBVcore18 (n=4); 7 individuals with NUC control/chronic HBV for HLA*02:01/HBVpol455 (n=4) and HLA*02:01/HBVcore18 (n=3) were sequenced and analysed in independent experiments (Fig. 1A-F; Ext. data Fig. 1B-D; Fig. 2A-D; Fig. 3A/B+E/F only HBVpol455 data; Ext. data Fig. 2A/D only HBVpol455 data; Ext. data Fig. 4A/B only HBVpol455 data; Ext. data Fig 6A+C).
Flow cytometry analysis:
26 individuals with endogenous control/chronic HBV for HLA*02:01/HBVpol455 (n=12) and HLA*02:01/HBVcore18 (n=14) and 25 individuals with NUC control/chronic HBV for HLA*02:01/HBVpol455 (n=14) and HLA*02:01/HBVcore18 (n=11) were analysed in independent experiments (Fig. 2E).
5-12 individuals with endogenous control/chronic HBV for HLA*02:01/HBVpol455, 7 for HLA*35:01/HBVpol173 and 5-14 for HLA*02:01/HBVcore18, 4 individuals with chronic HBV/high VL for HLA*02:01/HBVpol455 and 2 for HLA*02:01/HBVcore18, and 9-14 individuals with NUC control/chronic HBV for HLA*02:01/HBVpol455, 7 for HLA*35:01/HBVpol173 and 11-12 for HLA*02:01/HBVcore18,were analysed in independent experiments (Fig. 3C/D; Ext data Fig. 2B/C).
5-24 individuals with endogenous control/chronic HBV for HLA*02:01/HBVpol455 and 14 for HLA*02:01/HBVcore18 , 3-7 individuals with acute HBV infection for HLA*02:01/HBVpol455 and 5 for HLA*02:01/HBVcore18 and 3-5 individuals with acute resolved HBV infection for HLA*02:01/HBVpol455 and 3 for HLA*02:01/HBVcore18 were analysed in independent experiments (Fig. 4A-D;F; Fig. 5C; Fig. 6H only endogenous control/chronic HBV and acute HBV pol455 data; Ext. data Fig 3A/B; Ext. data Fig 4C/D/E; Ext. data Fig. 5B; Ext. data Fig 8D).
Ex vivo capacity to produce IFNγ, TNF or to degranulate in response to PMA/Ionomycin stimulation was tested in independent experiments with 6 individuals with endogenous control/chronic HBV for HLA*02:01/HBVpol455, 5 individuals with acute HBV infection for HLA*02:01/HBVpol455 and 6 individuals with acute resolved HBV infection for HLA*02:01/HBVpol455 (Fig. 4E).
GZMB+ HBV-specific CD8+ T cells were analysed for 12 individuals with endogenous control/chronic HBV for HLA*02:01/HBVpol455, 7 individuals with acute HBV infection for HLA*02:01/HBVpol455 and 4 individuals with acute resolved HBV infection for HLA*02:01/HBVpol455 in independent experiments (Fig. 5D/E; Ext. data Fig. 5A).
TGFβ signalling blockade assay was performed for 6 individuals with endogenous control/chronic HBV for HLA*02:01/HBVpol455 and 4 individuals with acute HBV infection for HLA*02:01/HBVpol455 in independent experiments (Fig 6C/H; Ext. data Fig. 6E/F; Ext. data Fig 7A/B; Ext. data Fig 8D).
Treatment of HBV pol455-specific CD8+ T cells with IL-12 or IFNα was performed for 6-8 individuals with endogenous control/chronic HBV for HLA*02:01/HBVpol455 in independent experiments (Fig. 6F/G/H; Ext. data Fig. 8B/C/D;).
scRNAseq analysis using 10x genomics platform:
3 individuals with endogenous control/chronic HBV for HLA*02:01/HBVpol455, 3 individuals with acute HBV infection for HLA*02:01/HBVpol455 and 2 individuals with acute resolved HBV infection for HLA*02:01/HBVpol455 were sequenced and analysed in two independent experiments. (Fig 5A/B,F; Fig 6A+B;Ext. data Fig. 4A/B; Ext. data Fig. 5C; Ext. data Fig 6D; Ext. data Fig 8A).
ELISA:
22 individuals with endogenous control/chronic HBV, 7 individuals with acute HBV infection and 5 individuals with acute resolved HBV infection were analysed for serum TGFβ concentration in independent experiments. (Ext. data Fig. 6G).

Randomization

Individuals within different clinical phases of chronic HBV infection as well as individuals with acute or acute resolved HBV infection were selected based on availability and HLA-typing. The covariates age and gender are well-documented: Median age of HLA-A*02:01-positive individuals with endogenous controlled chronic HBV infection was 38 years and gender ratio was m/f: 29/14. Median age of HLA-A*35:01-positive individuals with endogenous controlled chronic HBV infection was 49 years and gender ratio was m/f: 2/5. Median age of HLA-A*02:01-positive individuals with chronic HBV/high VL was 41.5 years and gender ratio was m/f: 5/5. Median age of HLA-A*35:01-positive HLA-A*02:01-positive individuals with NUC control/chronic HBV was 55 years and gender ratio was m/f: 18/9. Median age of HLA-A*35:01-positive HLA-A*35:01-positive individuals with NUC control/chronic HBV was 52 years and gender ratio was m/f: 4/3. HLA-A*02:01-positive individuals with acute HBV infection was 41 years and gender ratio was m/f: 7/1. HLA-A*02:01-positive individuals with acute resolved HBV infection was 52 years and gender ratio was m/f: 8/3.

Blinding

Blinding was not applied. Non-objective parameters were not included in the study design. Due to standardized analyses of the flow cytometric data set, biased analysis can be excluded.

Reporting for specific materials, systems and methods

We require information from authors about some types of materials, experimental systems and methods used in many studies. Here, indicate whether each material, system or method listed is relevant to your study. If you are not sure if a list item applies to your research, read the appropriate section before selecting a response.

Materials & experimental systems

n/a	Involved in the study
☐	☒ Antibodies
☒	☐ Eukaryotic cell lines
☒	☐ Palaeontology and archaeology
☒	☐ Animals and other organisms
☒	☐ Clinical data
☒	☐ Dual use research of concern
☒	☐ Plants

Methods

n/a	Involved in the study
☒	☐ ChIP-seq
☐	☒ Flow cytometry
☒	☐ MRI-based neuroimaging

Antibodies

Antibodies used

anti-CD14-APC-eFluor780 (61D3, 1:100) eBioscience 47-0149-42; LOT:2488593
anti-CD19- APC-eFluor780 (HIB19, 1:100) eBioscience 47-0199; LOT: 2472560
anti-EOMES- PE-Cy5.5 (WD1928, 1:800) eBioscience 35-4877-42; LOT:2313113
anti-KLRG1-Super Bright 702 (13F12F2, 1:50) eBioscience 67-9488-42; LOT: 2254207
anti-T-BET-PE-Cy7 (4B10, 1:200) eBioscience 25-5825; LOT: 2410093
anti-TOX-eFluor660 (TRX10, 1:100) eBioscience 50-6502; LOT: 2399962
anti-BLIMP1-PE-Dazzle (6D3, 1:25) BD Bioscience 565274; LOT:2158078
anti-CD107a-APC (H4A3, 1:100) BD Bioscience 560664; LOT:2320582
anti-CD28 - pure (CD28.2; 0.5 µg/ml) BD Bioscience 555726; LOT: 3065396
anti-CD38-BUV737 (HB7, 1:200) BD Bioscience 564686; LOT: 8339566
anti-CD45RA-BUV496 (HI100,1:200) BD Bioscience 750258; LOT: 2327528
anti-CD8-BUV496 (RPA-T8, 1:00) BD Bioscience 612942; LOT: 2213972
anti-CD8-BUV395 (RPA-T8,1:200) BD Bioscience 563795; LOT: 3237761
anti-CD8-BB515 (RPA-T8,1:100) BD Bioscience 564526; LOT: 2070054
anti-GZMB-BV510 (GB11, 1:100) BD Bioscience 563388; LOT: 3317967
anti-IFNγ-FITC (4S.B3, 1:8) BD Bioscience 340449; LOT: 3303149
anti-Ki67-BV510 (B56, 1:20) BD Bioscience 563462; LOT: 1018522
anti-KLRD1-BV421 (HP-3D9, 1:200) BD Bioscience 743948; LOT: 2201389
anti-TNF-PE-Cy7 (MAb11, 1:50) BD Bioscience 557647; LOT: 2131650
anti-PD1-BV786 (EH12.1, 1:33) BD Bioscience 563789; LOT: 3276824
anti-CCR7-Ax700 (G043H7, 1:25) BioLegend 353244; LOT: B387901
anti-CCR7 BV786 (G043H7, 1:33) BioLegend 353230; LOT: B372034
anti-CD127-BV605 (A019D5, 1:33) BioLegend 351334; LOT: B382456
anti-CD45RA BV510 (HI100, 1:200) BioLegend 304142; LOT: B309815
anti-Rabbit IgG- FITC (Poly4064, 1:200) BioLegend 406416; LOT: B341211
anti-Rabbit IgG- PE-CF594 (Poly4064, 1:200) BioLegend 406418; LOT: B360249
anti-PRF1-BV711 (dG9, 1:200) BioLegend 308130; LOT: B310140
anti-ZEB2-AF647 (923328, 1:25) R&D IC73782R; LOT: 1654618
anti-NKG7-pure (polyclonal, 1:50) Biorybt orb355831; LOT: DR7769
anti-RUNX1/2/3-pure (SD0803, 1:800) Thermofisher MA5-32373; LOT: WD3259036
Viability Dyes APC-eFluor780 (1:200) eBioscience 65-0865; LOT: 2594485
anti-PE microbeads (1:10) Miltenyi Biotec 130-048-801; LOT: 5240300312

Validation

All antibodies were obtained from commercial cendors and we based specificity on descriptions and information provided in corresponding data sheets available and provided by the manufacturers. Standardized analysis in different cohorts, antibody titration on PBMCs including unstained controls, comparisons of different antibody clones and conjugates and va Validation
antibody titration on PBMCs; control clones M5E2; using T cell populations as negative control
antibody titration on PBMCs; control clone SJ25C1; using T cell populations as negative control
antibody titration on PBMCs; validated with respect to differential expression of naïve and non-naïve T cell subpopulations
antibody titration on PBMCs; validated with respect to differential expression of naïve and non-naïve T cell subpopulations
antibody titration on PBMCs; control clones O4-46; validated with respect to differential expression of naïve and non-naïve T cell subpopulations
antibody titration on PBMCs; control clone REA473; validated with respect to differential expression of naïve and non-naïve T cell subpopulations
antibody titration on PBMCs; control clone C-21; validated with respect to differential expression of naïve and non-naïve T cell subpopulations
antibody titration on PBMCs; validated with respect to differential expression of activated and non-activated T cell subpopulation
antibody titration on PBMCs; control clone HIT2.1; validated with respect to differential expression of naïve and non-naïve T cell subpopulations
antibody titration on PBMCs; validated with respect to differential expression of naïve and non-naïve T cell subpopulations

antibody titration on PBMCs; control clone SK1; using B cells as negative control
antibody titration on PBMCs; control clone SK1; using B cells as negative control
antibody titration on PBMCs; control clone SK1; using B cells as negative control
antibody titration on PBMCs; polyclonal antibody as control; validated with respect to differential expression of activated and non-activated T cell subpopulations
antibody titration on PBMCs; control clone 4S.B3; validated with respect to differential expression of activated and non-activated T cell subpopulations
antibody titration on PBMCs; control clone Ki67; validated with respect to differential expression of naïve and non-naïve T cell subpopulations
antibody titration on PBMCs; control clone HP-3D9; validated with respect to differential expression of naïve and non-naïve T cell subpopulations
antibody titration on PBMCs; validated with respect to differential expression of activated and non-activated T cell subpopulations
antibody titration on PBMCs; control clone eBioJ105; validated with respect to differential expression of naïve and non-naïve T cell subpopulations
antibody titration on PBMCs; control clone 3D1; validated with respect to differential expression of naïve and non-naïve T cell subpopulations
antibody titration on PBMCs; control clone 3D1; validated with respect to differential expression of naïve and non-naïve T cell subpopulations
antibody titration on PBMCs; control clone HIL-7R-M21; validated with respect to differential expression of naïve and non-naïve T cell subpopulations
antibody titration on PBMCs; validated with respect to differential expression of naïve and non-naïve T cell subpopulations
antibody titration on PBMCs; validated with respect to differential expression of naïve and non-naïve T cell subpopulations
antibody titration on PBMCs; validated with respect to differential expression of naïve and non-naïve T cell subpopulations
antibody titration on PBMCs; control clone B-D48; validated with respect to differential expression of naïve and non-naïve T cell subpopulations
antibody titration on PBMCs; validated with respect to differential expression of naïve and non-naïve T cell subpopulations
antibody titration on PBMCs; validated with respect to differential expression of naïve and non-naïve T cell subpopulations
antibody titration on PBMCs; validated with respect to differential expression of naïve and non-naïve T cell subpopulations
Viability Dye was titrated on PBMCs; validated with respect to differential staining of live and dead cell populationslidated by publications.

Plants

Seed stocks
Report on the source of all seed stocks or other plant material used. If applicable, state the seed stock centre and catalogue number. If plant specimens were collected from the field, describe the collection location, date and sampling procedures.

Novel plant genotypes
Describe the methods by which all novel plant genotypes were produced. This includes those generated by transgenic approaches, gene editing, chemical/radiation-based mutagenesis and hybridization. For transgenic lines, describe the transformation method, the number of independent lines analyzed and the generation upon which experiments were performed. For gene-edited lines, describe the editor used, the endogenous sequence targeted for editing, the targeting guide RNA sequence (if applicable) and how the editor was applied.

Authentication
Describe any authentication procedures for each seed stock used or novel genotype generated. Describe any experiments used to assess the effect of a mutation and, where applicable, how potential secondary effects (e.g. second site T-DNA insertions, mosiacism, off-target gene editing) were examined.

Flow Cytometry

Plots

Confirm that:

☒ The axis labels state the marker and fluorochrome used (e.g. CD4-FITC).

☒ The axis scales are clearly visible. Include numbers along axes only for bottom left plot of group (a 'group' is an analysis of identical markers).

☒ All plots are contour plots with outliers or pseudocolor plots.

☒ A numerical value for number of cells or percentage (with statistics) is provided.

Methodology

Sample preparation
Cryopreserved isolated human PBMCs were thawed and prepared for multiparametric flow cytometry analysis (including magnetic bead based enrichment), in vitro expansion or FACS sorting for scRNA-seq experiments as described in the methods section.

Instrument
FACSCanto II, LSRFortessa (BD, Germany)

Software
FlowJo_v10.6.2 (Treestar), R version 4.3.3 using the Bioconductor (version: Release (3.18))

Cell population abundance
Abundance of HBV-specific T cells are low ($<10^{-4}$ %)

Gating strategy
CD8+ T cells: Lymphocytes gated on FSC-A and SSC-A, Doublet exclusion on FSC-A and FSC-H and FSC-A and FSC-W, Exclusion

Gating strategy

of dead cells, B cells and monocytes, Gating on CD8+ cells, Exclusion of naive cells (CCR7+CD45RA+), Gating of HBV-specific CD8+ T cells via tetramers described in methods part.

☒ Tick this box to confirm that a figure exemplifying the gating strategy is provided in the Supplementary Information.